

On Approximating the Dynamic Response of Synchronous Generators via Operator Learning: A Step Towards Building Deep Operator-based Power Grid Simulators

Christian Moya, Guang Lin, Tianqiao Zhao, and Meng Yue

January 31, 2023

Abstract

This paper designs an Operator Learning framework to approximate the dynamic response of synchronous generators. One can use such a framework to (i) design a neural-based generator model that can interact with a numerical simulator of the rest of the power grid or (ii) shadow the generator’s transient response. To this end, we design a data-driven Deep Operator Network (DeepONet) that approximates the generators’ infinite-dimensional solution operator. Then, we develop a DeepONet-based numerical scheme to simulate a given generator’s dynamic response over a short/medium-term horizon. The proposed numerical scheme recursively employs the trained DeepONet to simulate the response for a given multi-dimensional input, which describes the interaction between the generator and the rest of the system. Furthermore, we develop a residual DeepONet numerical scheme that incorporates information from mathematical models of synchronous generators. We accompany this residual DeepONet scheme with an estimate for the prediction’s cumulative error. We also design a data aggregation (DAGger) strategy that allows (i) employing supervised learning to train the proposed DeepONets and (ii) fine-tuning the DeepONet using aggregated training data that the DeepONet is likely to encounter during interactive simulations with other grid components. Finally, as a proof of concept, we demonstrate that the proposed DeepONet frameworks can effectively approximate the transient model of a synchronous generator.

1 Introduction

The smart grid [4] –the next generation of power grids– holds the significant promise of making electricity production and delivery more reliable and cost-effective. To achieve such a promise, the smart grid must enable and support multiple innovative technologies, including a growing fleet of electric vehicles, a vast number of distributed renewable energy resources, and an increasing number of responsive loads. To support these innovative technologies, the power systems community must design and develop new state-of-the-art methods for operating, predicting, and controlling the smart grid [17].

Over many decades, the power systems community has developed sophisticated numerical time-domain simulation schemes [28, 41] for predicting the power grid’s transient dynamic response. In particular, these schemes solve, with high-computational cost, the differential and algebraic equations (DAEs) describing the power grid after a disturbance event [28]. However, as the power grid becomes more innovative, power utilities have recognized the more significant need [15] to develop faster simulation tools to better understand and control the dynamics of the smart grid. For such tasks, which often require many complex forward simulations, the current state-of-the-art numerical time-domain simulation schemes may be prohibitively expensive.

1.1 Prior Works

Power grid time-domain simulation. Most commercial power grid simulators implement a partitioned-solution approach [28] or an implicit integration scheme. On the one hand, the partition approach sequentially solves DAEs describing the power grid dynamics. In particular, this approach freezes the dynamic (resp. algebraic) variables to solve for the algebraic (resp. dynamic) variables. Such a strategy enables independently simulating power grid dynamic components. However, it also introduces a delay error propagating throughout the power grid simulation [44]. On the other hand, implicit integration schemes simultaneously solve the differential and algebraic equations describing the power grid dynamics. Such a scheme eliminates delay error propagation. However, it requires simultaneously solving all the power grid components using expensive iterative methods (*e.g.*, Newton’s method), which may require matrix inversion [28].

Parallel computing-based solutions. Building on the continuous advance of high-performance parallel computing, many works [43, 45, 19, 33, 12, 3, 14, 16, 34] have proposed and developed parallel computing-based solutions to accelerate the simulation of complex power grids. For example, in [33], the authors employed high-performance computing to achieve faster simulation. Furthermore, the authors of [43, 45, 19] designed parallel algorithms for power grid dynamic simulation by spatially decomposing the simulation task. Similarly, one can also parallelize across (i) the time-domain [16, 34] or (ii) across numerical solvers [12, 3, 14]. In particular, the parareal in time algorithm was employed in [16, 34] to provide faster simulations of large-scale power grids. Parallel computing-based solutions, however, still consume a high amount of computational resources and the speedup is limited by the part of serial applications, which could prevent their application for tasks requiring multiple forward simulations, *e.g.*, control, uncertainty quantification, and optimization.

Deep learning-based solutions. Deep learning-based computational tools promise to transform how we predict and simulate complex dynamical systems. Thus, a recent wave of publications has provided encouraging results in the form of faster alternatives to traditional numerical schemes. These publications can be roughly classified into deep learning-based methods aiming at (i) learning the governing equations of the system [6, 7, 42], (ii) encoding the underlying physics into training protocols [39, 30, 20], or (iii) predicting the future states of the system [37, 36, 38]. For instance, Brunton *et al.* [6] used data to learn the unknown governing equations of a dynamic system. The authors then extended this work to learn a control dynamical system’s input/state governing equation [7]. Similarly, the authors of [42] used data to learn a sparse approximation of partial differential equations. For power grids, in [29], the authors employed the physics-informed neural network framework introduced in [39, 20] to encode a simplified version of the power grid’s dynamics into the training loss function. In our previous work [30], we designed a discrete physics-informed neural network that incorporates into training protocols stiff and differential-algebraic equations, which often describe the power grid dynamics.

On the other hand, many works [37, 36, 38] have proposed learning the system’s next-step response and recursively using this response to predict the system’s evolution for longer time horizons. One can implement such a next-step strategy using, for example, recurrent, residual networks (resNet) [37] or feed-forward neural networks [38]. However, most of the above deep learning-based methods avoid overfitting using vast amounts of data. Moreover, they likely require retraining when dealing with unseen operating conditions. As a result, the effective design of deep learning-based solutions for predicting and simulating large-scale complex dynamical systems is still a widely-open research question.

Component-based learning. To enable effective learning strategies for large-scale dynamical systems, one can follow a distributed (or component-based) design approach that requires learning

the input/output response of individual components. Then, by synchronizing the trained components, one can predict and simulate large-scale dynamical systems. In [25], we introduced this component-based learning strategy for the power systems community. Here, we used recurrent neural networks to approximate the input/output response of a synchronous generator (SG) interacting with the rest of the grid. The proposed strategy, however, (i) required a vast amount of data to control error propagation and (ii) needed a uniform simulation step size.

In a parallel effort, the authors of [1] proposed using continuous-time echo state networks for building a faster surrogate neural architecture. Such an architecture can (i) approximate the input/output response of a library of components and (ii) discretely interact with causal models through functional mockup interfaces [5]. The proposed architecture, however, ignores the problem’s infinite-dimensional nature, lacks the mathematical foundation of the original echo state networks [2], and needs rolling a numerical integration scheme to obtain the current prediction. To tackle the above drawbacks, in this paper, we propose using the mathematically-sound infinite-dimensional framework of operator learning, which we introduced to the power systems community in [32].

Operator learning. In the seminal paper [27], Lu *et al.* designed based on the universal approximation theorem for nonlinear operators [9] a Deep Operator Network (DeepONet) framework, which can learn nonlinear operators (*i.e.*, mappings between infinite-dimensional spaces). Compared to traditional neural networks, the proposed DeepONet learns with streams of scattered data and exhibits minor generalization errors, as demonstrated in applications such as control systems [24], power systems [32], or multi-physics problems [8]. Extensions to the original DeepONet framework have enabled dealing with stiff dynamics [46] and discontinuities [23], incorporating physics-informed training [46], and quantifying uncertainty [32, 26, 50]. Thus, in this paper, we adopt an operator learning framework to design an efficient and effective deep operator network, which learns the solution operator of power grid dynamic components (*e.g.*, SGs) interacting with the rest of a power grid (*e.g.*, represented via a numerical simulator).

1.2 Our Work

The objectives of this paper are described next.

1. *Learning the solution operator.* We aim to design a deep operator learning framework to approximate the local solution operator of non-autonomous systems. Such an operator can describe the dynamic response of a library of grid components (*e.g.*, SGs) interacting with the rest of a power grid for any given local time interval.
2. *Short- and medium-term simulation.* We aim to design a recursive numerical scheme that uses the proposed framework to predict the dynamic response of SGs to a distribution of operating conditions.
3. *Incorporating power grid’s mathematical models.* We aim to incorporate into our framework information from the mathematical models the power systems community has developed over many decades.

We detail the contributions of this paper next.

- First, we design (in Section 3) a Deep Operator Network (DeepONet) that approximates the local solution operator of an SG. Our DeepONet takes as inputs (i) the current state, (ii) the current interface input describing the interaction of the generator with the rest of a power grid, and (iii) an arbitrary prediction step. The DeepONet then outputs the desired

future state over an arbitrary time interval. To the best of our knowledge, this is the first time operator learning has been used to approximate the solution operator corresponding to dynamic components of the power grid.

- We then (in Section 3.2) develop a DeepONet-based numerical scheme that recursively uses the trained DeepONet to simulate the generator’s dynamic response over a given short/medium-term horizon.
- Furthermore, we design (in Section 4) a residual DeepONet framework that learns the residual dynamics resulting from comparing the actual solution operator with the solution operator obtained from (i) an *available* mathematical model describing the generator or (ii) a trained physics-informed neural network.
- We provide (in Section 4.3) a theoretical estimate of the cumulative error obtained when employing the proposed residual DeepONet numerical scheme.
- For the case of a generator interacting with a numerical simulator of the rest of the grid, we design (in Section 5) a data aggregation (Dagger) algorithm that enables the (i) supervised training of DeepONets with relatively small datasets and (ii) fine-tuning of DeepONets by aggregating datasets that the trained DeepONet will likely encounter when interacting with the numerical simulator.
- As a proof of concept, we demonstrate (in Section 6) the efficacy of the proposed DeepONet framework by approximating a transient model of an SG that interacts with a power grid modeled as an infinite bus.

We remark that the methods developed in this paper for SGs can also be used for other dynamic components of the power distribution and transmission systems such as inverter-based generators (IBGs).

We organize the rest of the paper as follows. First, in Section 2, we describe the problem of approximating the solution operator of an SG interacting with a power grid. Then, Section 3 presents a data-driven DeepONet that learns this solution operator locally. Using the trained DeepONet, we detail in Section 3.2 a DeepONet-based scheme that simulates/predicts the component’s dynamic response over a given short/medium-term horizon. In Section 4, we design and estimate the cumulative error of a residual DeepONet framework that learns to use available mathematical models of SGs. Section 5 designs a data aggregation (Dagger) for training and fine-tuning DeepONets. As a proof of concept, we illustrate in Section 6 the efficacy of the proposed frameworks by learning a transient model of a synchronous generator. Finally, Section 7 discusses our results and future work, and Section 8 concludes the paper.

2 Problem Formulation

This paper aims to approximate the dynamic response of a synchronous generator interacting with a power grid (*e.g.*, a reduced power grid model or a numerical simulator such as power systems toolbox (PST) [10]). We model such a generator using the following non-autonomous initial value problem (IVP):

$$\begin{aligned} \frac{d}{dt}x(t) &= f(x(t), y(t), u(t); \lambda), & t \in [0, T], \\ x(0) &= x_0. \end{aligned} \tag{1}$$

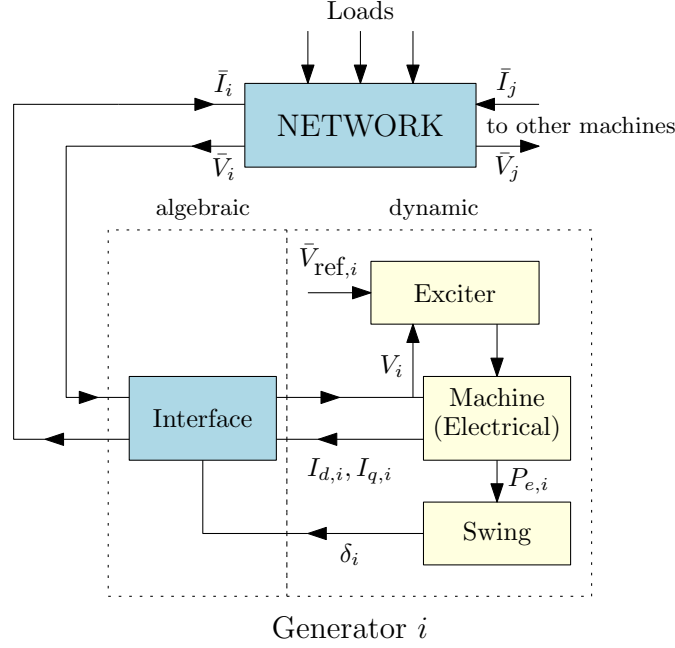


Figure 1: A *block diagram* description of the differential-algebraic model (2) introduced in [41]. The model describes the Network equations (2c), the stator (*i.e.*, generator interface) algebraic equations (2b), and the SGs' differential equations (2a).

Here $x(t) \in \mathcal{X} \subseteq \mathbb{R}^{n_x}$ is the vector-valued state function, $y(t) \in \mathcal{Y} \subseteq \mathbb{R}^{n_y}$ the interacting variables, $u(t) \in \mathcal{U} \subseteq \mathbb{R}^{n_u}$ the control input, $\lambda \in \Lambda \subset \mathbb{R}^{n_\lambda}$ the vector of parameters describing a specific generator, $[0, T] \subset [0, +\infty)$ the finite time horizon of interest, and $x_0 \in \mathcal{X}$ is the initial condition. We will assume the vector field $f : \mathcal{X} \times \mathcal{Y} \times \mathcal{U} \rightarrow \mathcal{X}$ is (i) unknown (in Section 3) and (ii) partially known (in Section 4), *i.e.*, we know some approximate model such that $f_{\text{approx}} \approx f$.

One can use the above non-autonomous IVP (1) to (i) describe the dynamic response of a synchronous generator that interacts with a numerical simulator, *e.g.*, PST (see Figure 1) or (ii) shadow the dynamic response of an actual generator. More specifically, consider a multi-machine power grid described using the following differential-algebraic (DA) model introduced in Sauer *et al.* [41]:

$$\dot{z} = f_o(z, I_{d-q}, \bar{V}, u) \quad (2a)$$

$$I_{d-q} = h(z, \bar{V}) \quad (2b)$$

$$0 = g(z, I_{d-q}, \bar{V}). \quad (2c)$$

In the above, (2a) are the synchronous generators' dynamic equations, (2b) the stator algebraic equations, and (2c) the network equations. Within this DA model, the proposed operator learning framework could provide the dynamic response of a *parametric family* of synchronous generators, *i.e.*, $f(\cdot; \lambda_i) \approx f_{o,i}$ for some i 's. In such a case, the interacting variables are (see Figure 1) the generator's stator currents and bus terminal voltage, *i.e.*, $y(t) = (I_d(t), I_q(t), V(t))^T$ and the control input is the voltage regulator field voltage, *i.e.*, $u(t) \equiv E_{fd}(t)$. We remark, however, that the proposed method can use other interacting variables. For example, bus active and reactive powers, which we used in our previous work [25].

Focusing on interacting variables. In this paper, we only focus on the interacting variables input $y(t)$, neglect the control input $u(t)$, and fix the parameters λ . This is because the analysis and learning protocols for $u(t)$ and λ , which we will extensively study in a separate work, are

similar to the analysis for $y(t)$. Furthermore, the interacting variables $y(t)$ propagate prediction errors when interacting with a numerical simulator for the rest of the grid. Thus, it is imperative to design robust deep-learning methods to control this error propagation. Without the control input $u(t)$, we write the dynamics of the non-autonomous IVP (1) as follows

$$\begin{aligned}\frac{d}{dt}x(t) &= f(x(t), y(t); \lambda), & t \in [0, T], \\ x(0) &= x_0.\end{aligned}\tag{3}$$

The solution operator. We describe the dynamic response of the selected generator using the *solution operator* (also known as flow map) of (3), which we denote as G . G takes as inputs the initial condition $x(0) = x_0 \in \mathcal{X}$ and the continuous sequence of interacting variables, which we denote, with some abuse of notation, as $y_{[0,t]} := \{y(s) \in \mathcal{Y} : s \in [0, t]\}$. G then computes the state $x(t) \in \mathcal{X}$ at time $t \in [0, T]$ as follows

$$G(x_0, y_{[0,t]}; \lambda)(t) \equiv x(t) = x_0 + \int_0^t f(x(s), y(s); \lambda) ds.$$

Approximate non-autonomous IVP. In practice, however, we may have only access to a discrete representation of the trajectory of $y(t)$ within the interval $[0, T]$. We denote such an approximation as \tilde{y} . Using \tilde{y} in (3) leads to the following approximate non-autonomous IVP:

$$\begin{aligned}\frac{d}{dt}\tilde{x}(t) &= f(\tilde{x}(t), \tilde{y}; \lambda), & t \in [0, T], \\ \tilde{x}(0) &= x_0,\end{aligned}\tag{4}$$

whose solution operator \tilde{G} is

$$\tilde{G}(x_0, \tilde{y}; \lambda)(t) \equiv \tilde{x}(t) = x_0 + \int_0^t f(\tilde{x}(s), \tilde{y}; \lambda) ds, \quad t \in [0, T].$$

In Lu *et al.* [27], the authors designed a Deep Operator Network (DeepONet) to approximate the solution operator G (with $x_0 = 0$) and proved its approximation capacity via \tilde{G} . The input to the proposed DeepONet was the trajectory of the function $y_{[0,T]}$ discretized using $m \geq 1$ interpolation points (also known as *sensors* in [27]). However, their proposed DeepONet [27] has the following *two* drawbacks. (i) Their DeepONet can effectively approximate G (with $x_0 = 0$) for small values of T . For longer time horizons, *i.e.*, for $T \gg 1$ second, one must increase the number m of sensors, which makes the training process challenging. (ii) To predict $x(t)$ for any $t \in [0, T]$, their DeepONet must take as input the trajectory $u(t)$ within *the whole* interval $[0, T]$. Such an assumption does not hold in the problem studied in this paper. That is, we only have access to past values of $y(t)$, *i.e.*, within the interval $[0, t] \subset [0, T]$. The DeepONet designed in [27] is not applicable to the problem we are addressing here.

To alleviate the above two drawbacks, we propose in the next section an operator learning framework that first designs and trains a novel DeepONet to approximate G locally and then uses the trained DeepONet recursively to approximate the generator's dynamic response over the whole interval $[0, T]$.

3 The Deep Operator Learning Framework

The proposed operator learning framework aims to approximate the *local* solution operator, *i.e.*, the solution operator G within the arbitrary time interval $[t_n, t_n + h_n] \subset [0, T]$:

$$\tilde{G}(\tilde{x}(t_n), \tilde{y}_m^n, \lambda)(h_n) \equiv \tilde{x}(t_n + h_n) = \tilde{x}(t_n) + \int_0^{h_n} f(\tilde{x}(t_n + s), \tilde{y}_m^n; \lambda) ds, \quad h_n \in (0, h],$$

where \tilde{y}_m^n is the *discretized* input $y(t)$ within the interval $[t_n, t_n + h_n]$ using $m \geq 1$ sensors, *i.e.*,

$$\tilde{y}_m^n = (y(t_n + d_0), y(t_n + d_1), \dots, y(t_n + d_{m-1})) \approx y_{[t_n, t_n + h_n]}.$$

In the above, $h_n \leq h$ is the step-size, $h > 0$ the given maximum step-size, and $\{d_{k-1}\}_{k=1}^m \subset [0, h_n]$ the relative sensor locations.

Remark. The case of $m = 1$ sensors. Let us consider an SG interacting with a numerical simulator. When the number of sensors is one, *i.e.*, when $m = 1$, the discretized interacting variable is the singleton $\tilde{y}_m^n \equiv y(t_n)$. Such a scenario resembles the integration step of the generator's dynamics within the partition-solution approach [28], which is (i) used, for example, in PST [10] and (ii) extensively implemented in our numerical experiments (Section 6).

3.1 The Deep Operator Network

To approximate the *local* solution operator, we draw inspiration from successful strategies used in the numerical analysis of partial differential equations [18]. That is, we approximate the solution operator using a *trainable* linear representation. In particular, the coefficients of the trainable linear representation will process the inputs $x(t_n)$ and \tilde{y}_m^n , and the corresponding basis functions will process location points h_n within the output function domain $[0, h]$. Such a linear model will lead to a novel multi-output *Deep Operator Network* (DeepONet) G_θ , with a vector of trainable parameters $\theta \in \mathbb{R}^p$. DeepONet consists of *two* neural networks (see Figure 2): the *Branch* Net and the *Trunk* Net.

The *Branch* Net takes as input (i) the current state $x(t_n) \in \mathcal{X}$ and (ii) the trajectory of interacting variable \tilde{y}_m^n discretized using $m \geq 1$ sensors. Then, the *Branch* Net outputs the vector of trainable coefficients $\beta \in \mathbb{R}^{qn_x}$.

To enable the recursive numerical scheme detailed in Section 3.2, we also need to design the *Branch* Net to be resolution-independent. That is, it must allow flexible locations for the m sensors. To this end, we allow the Branch Net to take as the input the concatenation of the vector of relative sensor locations $\{d_{k-1}\}_{k=1}^m \subset [0, h_n]$ with the input values \tilde{y}_m^n , as depicted in Figure 2. However, we remark that for the critical case of $m = 1$, *i.e.*, when we use the partition approach [28], one does not need to include the relative sensor location.

The *Trunk* Net takes as input the step-size $h_n \in (0, h_n]$ and outputs the vector of trainable basis functions:

$$\varphi := (\varphi_1(h_n), \varphi_2(h_n), \dots, \varphi_{qn_x}(h_n))^\top \in \mathbb{R}^{qn_x}.$$

Finally, we compute each component of the DeepONet's vector output (*i.e.*, each predicted state), $G_\theta(x(t_n), \tilde{y}_m^n, \lambda)(h_n) \equiv x(t_n + h_n)$, using a linear representation (*i.e.*, via the dot product):

$$x^{(i)}(t_n + h_n) \equiv G_\theta^{(i)}(x(t_n), \tilde{y}_m^n; \lambda)(h_n) = \sum_{j=1}^q \beta_{(i-1)q+j} (x(t_n), \tilde{y}_m^n) \cdot \varphi_{(i-1)q+j}(h_n).$$

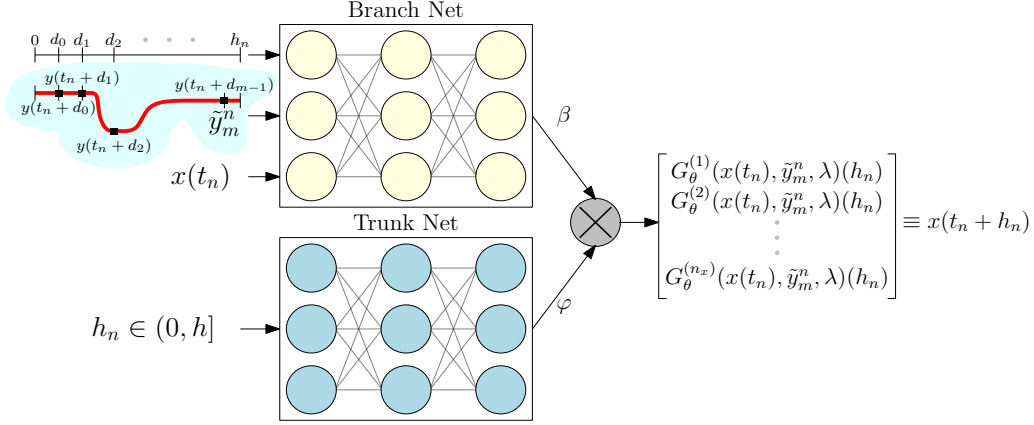


Figure 2: The DeepONet for learning the solution operator describing the dynamic response of an SG. The Branch Net takes as input a vector resulting from concatenating (i) the current state $\tilde{x}(t_n) \in \mathbb{R}^{n_x}$, (ii) the discretized interacting variables $\tilde{y}_m^n \in \mathbb{R}^m$, and (iii) the relative/flexible sensor locations $\{d_{k-1}\}_{k=1}^m \subset [0, h_n]$. Then, the Branch Net outputs the vector of trainable coefficients $\beta \in \mathbb{R}^{q_{n_x}}$. The Trunk Net takes as the input $h_n \in (0, h]$ and outputs the vector of trainable basis functions $\varphi \in \mathbb{R}^{q_{n_x}}$. Finally, we obtain the DeepONet's output using *linear trainable approximations of the states*, i.e., a dot product between β and φ .

Remark. The incremental solution operator. An alternative approach for approximating the local solution operator G is to build a DeepONet G_θ , which approximates the following incremental solution operator within the interval $[t_n, t_n + h_n]$:

$$\tilde{G}_\Delta(\tilde{x}(t_n), \tilde{y}_m^n, \lambda)(h_n) \equiv \tilde{x}(t_n + h_n) - x(t_n) = \int_0^{h_n} f(\tilde{x}(t_n + s), \tilde{y}_m^n; \lambda) ds, \quad h_n \in (0, h],$$

and then recover the solution operator G using:

$$G \approx G_\theta(\tilde{x}(t_n), \tilde{y}_m^n, \lambda)(h_n) + x(t_n).$$

We have empirically tested both approaches, and they lead to similar experimental results. However, using the incremental operator reduces the training effort of DeepONets.

Training the DeepONet. To train the vector of parameters $\theta \in \mathbb{R}^p$, we minimize the loss function:

$$\mathcal{L}(\theta; \mathcal{D}_{\text{train}}) = \frac{1}{N_{\text{train}}} \sum_{k=1}^{N_{\text{train}}} \left\| \tilde{G}_{*,k} - G_\theta(x_k(t_n), \tilde{y}_{m,k}^n, \lambda_k)(h_{n,k}) \right\|_2^2,$$

using the dataset of $N_{\text{train}} := |\mathcal{D}_{\text{train}}|$ triplets:

$$\mathcal{D}_{\text{train}} := \left\{ (x_k(t_n), \tilde{y}_{m,k}^n, h_{n,k}, \tilde{G}_{*,k}) \right\}_{k=1}^{N_{\text{train}}}.$$

where $\tilde{G}_* = \tilde{G} \equiv x(t_n + h_n)$ for the solution operator and $\tilde{G}_* = \tilde{G}_\Delta \equiv x(t_n + h_n) - x(t_n)$ for the incremental solution operator.

3.2 Predicting the Dynamic Response over the Interval $[0, T]$

To predict the dynamic response of the selected device, *e.g.*, a synchronous generator, we propose the *recursive* DeepONet-based numerical scheme described in Algorithm 1.

Algorithm 1: DeepONet-based Numerical Scheme

- 1 **Require:** trained DeepONet G_{θ^*} , device's parameters $\lambda \in \Lambda$, initial state $x_0 \in \mathcal{X}$, and time partition $\mathcal{P} \subset [0, T]$.
 - 2 Initialize $\tilde{x}(t_0) = x_0$
 - 3 **for** $n = 0, \dots, M - 1$ **do**
 - 4 observe the local trajectory of interacting variables \tilde{y}_m^n
 - 5 update the independent variable $t_{n+1} = t_n + h_n$
 - 6 update the state vector with the forward pass of DeepONet
$$\tilde{x}(t_{n+1}) = G_{\theta^*}(\tilde{x}(t_n), \tilde{y}_m^n, \lambda)(h_n).$$
 - 7 **end**
 - 8 **Return:** simulated trajectory $\{\tilde{x}(t_n) \in \mathcal{X} : t_n \in \mathcal{P}\}$.
-

Algorithm 1 takes as inputs (i) the trained DeepONet G_{θ^*} , (ii) the corresponding fixed generator's parameters $\lambda \in \Lambda$, (3) the initial condition $x_0 \in \mathcal{X}$, and (4) the arbitrary time partition $\mathcal{P} \subset [0, T]$ of size M defined as follows:

$$\mathcal{P} : 0 = t_0 < t_1 < \dots < t_M = T,$$

where the n th step-size, $h_n := t_{n+1} - t_n \in (0, h]$, is arbitrary. Then, during the n th recursive step of the algorithm, the DeepONet observes (i) the current state $\tilde{x}(t_n) \in \mathcal{X}$, (ii) the step-size h_n , and (iii) the local discretized input of interacting variables \tilde{y}_m^n to update the state vector, *i.e.*, to compute $\tilde{x}(t_{n+1})$. The final output from Algorithm 1 is the simulated trajectory $\{\tilde{x}(t_n) \in \mathcal{X} : t_n \in \mathcal{P}\}$.

We conclude this section with two remarks. First, we can estimate the cumulative error associated with Algorithm 1. We leave such an estimation for our future work. Second, the DeepONet proposed in this section is entirely data-driven; hence, it can exploit the increase of data available from power grids. However, the power engineering community has spent decades developing sophisticated mathematical models to represent dynamic components in power systems. As a result, in the next section, we will design a DeepONet framework that can use the data and incorporate mathematical models to predict the dynamic response of synchronous generators.

4 Incorporating Power Grid Mathematical Models

On the one hand, the amount of data collected by utilities has increased during the last few years. On the other hand, the power engineering community has developed and optimized sophisticated first-principle mathematical models for planning, operating, and controlling the power grid. Thus, we believe our proposed DeepONet framework must be able to (i) learn from high-fidelity datasets and (ii) use previously developed mathematical models.

To this end, in this section, we propose a residual DeepONet –a deep operator network that approximates the residual (or error correction) operator. This residual operator describes the error/residual dynamics between the component's true solution operator \hat{G} and the solution operator resulting from the component's mathematical model.

Formally, we consider the following non-autonomous IVP based on the previously derived math-

emational model of an SG:

$$\begin{aligned}\frac{d}{dt}\tilde{x}(t) &= f_{\text{approx}}(\tilde{x}(t), \tilde{y}; \lambda), \quad t \in [0, T], \\ \tilde{x}(0) &= x_0.\end{aligned}\tag{5}$$

In the above, $f_{\text{approx}} : \mathcal{X} \times \mathcal{Y} \rightarrow \mathcal{X}$ is the known vector field that approximates the true vector field f , *i.e.*, $f_{\text{approx}} \approx f$ of a synchronous generator. The corresponding *local* solution of (5) is

$$\tilde{G}_{\text{approx}}(\tilde{x}(t_n), \tilde{y}_m^n, \lambda)(h_n) \equiv \tilde{x}(t_n) + \int_0^{h_n} f_{\text{approx}}(\tilde{x}(t_n + s), \tilde{y}_m^n; \lambda) ds, \quad h_n \in (0, h].$$

In practice, we may only have access to this approximate representation of the solution operator, which we denote as \hat{G}_{approx} . \hat{G}_{approx} can be, for example, (i) a step of an integration scheme, *e.g.*, Runge-Kutta [18], with variable step-size h_n , (ii) a physics-informed DeepONet [46] trained to satisfy (5) locally, or (iii) a DeepONet (see Section 3) trained using a dataset \mathcal{D} generated by simulating (5).

Inspired on multi-fidelity schemes [21, 49], we propose to decompose the local solution operator \tilde{G} as follows:

$$\begin{aligned}\tilde{G}(\tilde{x}(t_n), \tilde{y}_m^n, \lambda)(h_n) &\equiv \tilde{x}(t_n + h_n) \\ &= \tilde{x}(t_n) + \int_0^{h_n} f(\tilde{x}(t_n + s), \tilde{y}_m^n, \lambda) ds \\ &= \tilde{x}(t_n) + \int_0^{h_n} f_{\text{approx}}(\tilde{x}(t_n + s), \tilde{y}_m^n, \lambda) ds + \text{“residual dynamics”} \\ &= \tilde{G}_{\text{approx}}(\tilde{x}(t_n), \tilde{y}_m^n, \lambda)(h_n) + \text{“residual dynamics”}.\end{aligned}$$

Thus, we define the *residual operator* G_ϵ as:

$$G_\epsilon(\tilde{x}(t_n), \tilde{y}_m^n, \lambda)(h_n) := [\tilde{G} - \tilde{G}_{\text{approx}}](\tilde{x}(t_n), \tilde{y}_m^n, \lambda)(h_n), \quad h_n \in (0, h].$$

In the above, we have adopted an affine decomposition of the true solution operator \tilde{G} . Such a decomposition will simplify the mathematical analysis of the cumulative error of the proposed residual DeepONet numerical scheme (see Section 4.3). However, we remark that other decomposition forms are also possible. For example, we can use the multi-fidelity framework [49]: $\tilde{G} = G_{\epsilon, \cdot} \circ \tilde{G}_{\text{approx}} + G_{\epsilon, +}$. Such a framework will be studied in our future work.

4.1 The Residual DeepONet Design

To approximate the residual operator G_ϵ , we design a residual deep operator network (residual DeepONet) G_θ^ϵ , with trainable parameters $\theta \in \mathbb{R}^p$. G_θ^ϵ has the same architecture as the data-driven DeepONet (see Figure 2). That is, G_θ^ϵ has a Branch Net and a Trunk Net with the same inputs. Furthermore, the residual DeepONet’s output, which we define as follows:

$$\begin{aligned}G^\epsilon(\tilde{x}(t_n), \tilde{y}_m^n, \lambda)(h_n) &:= \tilde{e}(t_n + h_n) \in \mathbb{R}^{n_x} \\ &= x(t_n + h_n) - \tilde{x}_{\text{approx}}(t_n + h_n) \\ &= [\tilde{G} - \tilde{G}_{\text{approx}}](\tilde{x}(t_n), \tilde{y}_m^n, \lambda)(h_n),\end{aligned}$$

is approximated using the same dot product as for the data-driven DeepONet case.

Algorithm 2: Residual DeepONet Numerical Scheme

```
1 Require: trained residual DeepONet  $G_{\theta^*}^\epsilon$ , device's parameters  $\lambda \in \Lambda$ , initial state  $x_0 \in \mathcal{X}$ ,  
   and time partition  $\mathcal{P} \subset [0, T]$ .  
2 Initialize  $\tilde{x}(t_0) = x_0$   
3 for  $n = 0, \dots, M - 1$  do  
4   observe the local trajectory of interacting variables  $\tilde{y}_m^n$   
5   update the independent variable  $t_{n+1} = t_n + h_n$   
6   solve (5) to obtain  $\tilde{x}_{\text{approx}}(t_{n+1}) = \tilde{G}_{\text{approx}}(\tilde{x}(t_n), \tilde{y}_m^n, \lambda)(h_n)$   
7   forward pass of the residual DeepONet  
    $\tilde{e}(t_{n+1}) = G_{\theta^*}^\epsilon(\tilde{x}(t_n), \tilde{y}_m^n, \lambda)(h_n)$   
8   update the state vector  
    $\tilde{x}(t_{n+1}) = \tilde{x}_{\text{approx}}(t_{n+1}) + \tilde{e}(t_{n+1})$   
9 end  
10 Return: simulated trajectory  $\{\tilde{x}(t_n) \in \mathcal{X} : t_n \in \mathcal{P}\}$ .
```

To train the parameters of G_θ^ϵ , we minimize the loss function:

$$\mathcal{L}(\theta; \mathcal{D}_{\text{train}}) = \frac{1}{N_{\text{train}}} \sum_{k=1}^{N_{\text{train}}} \left\| \tilde{e}_k(t_n + h_{n,k}) - G_\theta^\epsilon(x_k(t_n), \tilde{y}_{m,k}^n, \lambda_k)(h_{n,k}) \right\|_2^2,$$

using the dataset of $N_{\text{train}} := |\mathcal{D}_{\text{train}}|$ triplets:

$$\mathcal{D}_{\text{train}} := \left\{ (x_k(t_n), \tilde{y}_{m,k}^n, h_{n,k}, \tilde{e}_k(t_n + h_{n,k})) \right\}_{k=1}^{N_{\text{train}}}.$$

4.2 Predicting the Dynamic Response over the Interval $[0, T]$

To predict the dynamic response of the generator over the interval $[0, T]$, we propose the recursive residual DeepONet numerical scheme detailed in Algorithm 2.

Algorithm 2 takes as inputs (i) the trained residual DeepONet $G_{\theta^*}^\epsilon$, (ii) the device's parameters $\lambda \in \Lambda$, (iii) the initial condition $x_0 \in \mathcal{X}$, and the time partition $\mathcal{P} \subset [0, T]$. During the n th recursive step of the algorithm, we (i) observe the current state $x(t_n)$ and the local discretized input of interacting variables \tilde{y}_m^n , (ii) solve (5) to obtain the approximate next state vector $\tilde{x}_{\text{approx}}(t_n + 1)$ (or use a trained physics-informed neural network), (iii) perform a forward pass of residual DeepONet $G_{\theta^*}^\epsilon$ to obtain the predicted error $\tilde{e}(t_{n+1})$, and (iv) update the state vector via $\tilde{x}(t_{n+1}) = \tilde{x}_{\text{approx}}(t_{n+1}) + \tilde{e}(t_{n+1})$. Finally, Algorithm 2 outputs the simulated trajectory $\{\tilde{x}(t_n) \in \mathcal{X} : t_n \in \mathcal{P}\}$. Let us conclude this section by providing next an estimate for the cumulative error of Algorithm 2.

4.3 Error Bound for the residual DeepONet Numerical Scheme

This section provides an estimate for the cumulative error bound between $x(t_n)$ obtained using the *true* solution operator and $\hat{x}(t_n)$ obtained using the residual DeepONet numerical scheme detailed in Algorithm 2. To this end, we start by stating the following assumptions.

Assumptions. We assume the interacting variables *input function* y belong to $V \subset C[0, T]$, where V is compact. We also assume the vector field $f : \mathcal{X} \times \mathcal{Y} \rightarrow \mathcal{X}$ is Lipschitz in x and y ,

i.e.,

$$\begin{aligned}\|f(x_1, y) - f(x_2, y)\| &\leq L\|x_1 - x_2\|, \\ \|f(x, y_1) - f(x, y_2)\| &\leq L\|y_1 - y_2\|,\end{aligned}$$

where $L > 0$ is a Lipschitz constant and x_1, x_2, y_1 and y_2 are in the proper space. Note that such assumptions are generally satisfied by engineering systems as f is often differentiable with respect to x and y . However, we will show empirically (see Section 6) that DeepONet can provide an accurate prediction even when the above assumptions fail, *e.g.*, when the external power grid to the synchronous generator experiences a disturbance.

We now provide in the following Lemma an estimate for the error bound between $x(t_n)$ obtained using the true solution operator and $\tilde{x}(t_n)$ obtained using the solution operator of the approximate model (4). For simplicity, we will assume y is a one-dimensional input. Extending our analysis to multiple inputs is straightforward.

Lemma 4.1. For any $t_n \in \mathcal{P}$ and $h_n \in (0, h]$, we have

$$\|x(t_n) - \tilde{x}(t_n)\| \leq \frac{1 - r^n}{1 - r} \mathcal{E}, \quad (6)$$

where $r := e^{Lh}$ and $\mathcal{E} := \max_n \{Lh_n \kappa_n e^{Lh_n}\}$.

Proof. For any $h_n \in (0, h]$,

$$\begin{aligned}x(t_{n+1}) &\equiv G(x(t_n), y, \lambda)(h_n) = x(t_n) + \int_{t_n}^{t_n+h_n} f(G(x(t_n), y, \lambda)(s), y(s)) ds, \\ \tilde{x}(t_{n+1}) &\equiv G(\tilde{x}(t_n), \tilde{y}, \lambda)(h_n) = \tilde{x}(t_n) + \int_{t_n}^{t_n+h_n} f(G(\tilde{x}(t_n), \tilde{y}, \lambda)(s), \tilde{y}(s)) ds.\end{aligned}$$

We then have

$$\begin{aligned}\|x(t_{n+1}) - \tilde{x}(t_{n+1})\| &\leq \|x(t_n) - \tilde{x}(t_n)\| + \int_{t_n}^{t_n+h_n} \|f(x(s), y(s)) - f(\tilde{x}(s), \tilde{y}, \lambda)(s), \tilde{y}(s))\| ds \\ &\leq \|x(t_n) - \tilde{x}(t_n)\| + L \int_{t_n}^{t_n+h_n} |y(s) - \tilde{y}(s)| ds + L \int_{t_n}^{t_n+h_n} \|x(s) - \tilde{x}(s)\| ds \\ &\leq \|x(t_n) - \tilde{x}(t_n)\| + Lh_n \kappa_n + L \int_{t_n}^{t_n+h_n} \|x(s) - \tilde{x}(s)\| ds.\end{aligned}$$

In the above, κ_n is the local approximation of the input y within the arbitrary interval $[t_n, t_n+h_n]$:

$$\max_{s \in [t_n, t_n+h_n]} |y(s) - \tilde{y}(s)| \leq \kappa_n$$

such that $\kappa \searrow 0$ as the number of sensors $m \nearrow +\infty$. We refer the interested reader to [27] for more details about the above input approximation. Then, using Gronwall's inequality we have

$$\|x(t_{n+1}) - \tilde{x}(t_{n+1})\| \leq \|x(t_n) - \tilde{x}(t_n)\| e^{Lh_n} + Lh_n \kappa e^{Lh_n}.$$

Taking $\mathcal{E} := \max_n \{Lh_n \kappa_n e^{Lh_n}\}$ gives

$$\|x(t_{n+1}) - \tilde{x}(t_{n+1})\| \leq \|x(t_n) - \tilde{x}(t_n)\| e^{Lh_n} + \mathcal{E}.$$

The bound (6) follows due to $x(t_0) = \tilde{x}(t_0) = x_0$. □

Before we estimate the cumulative error between $\tilde{x}(t_n)$ obtained using the solution operator of the approximate model (4) and $\hat{x}(t_n)$ obtained using the proposed residual DeepONet numerical scheme, we must first review the universal approximation theorem of neural networks for high-dimensional functions introduced in [13]. For a given $h_n \in (0, h]$, define the following vector-valued continuous function $\varphi : \mathbb{R}^{n_x} \times \mathbb{R}^m \times \mathbb{R}^{n_p} \rightarrow \mathbb{R}^{n_x}$

$$\varphi(z_n, \tilde{y}_m^n, \lambda) = [G - G_{\text{approx}}](z_n, \tilde{y}_m^n, \lambda)(h_n),$$

where $z_n \in \mathbb{R}^{n_x}$. Then, by the universal approximation theorem, for $\epsilon > 0$, there exists $W_1 \in \mathbb{R}^{K \times (n_x + m + n_p)}$, $b_1 \in \mathbb{R}^K$, $W_2 \in \mathbb{R}^{n_x \times K}$, and $b_2 \in \mathbb{R}^{n_x}$ such that

$$\|\varphi(z_n, \tilde{y}_m^n, \lambda) - G_{\theta^*}^\epsilon(z_n, \tilde{y}_m^n, \lambda)\| < \epsilon, \quad (7)$$

where

$$G_{\theta^*}^\epsilon(z_n, \tilde{y}_m^n, \lambda) =: (W_2 \sigma(W_1 \cdot \text{col}(z_n, \tilde{y}_m^n, \lambda) + b_1) + b_2).$$

We now introduce the following Lemma, presented in [36], provides an alternative form to describe the local solution operator G of the approximate system (4).

Lemma 4.2. Consider the local solution operator of the approximate model (4), *i.e.*, $G(\tilde{x}(t_n), \tilde{y}_m^n, \lambda)(h_n)$. Then, there exists a function $\Phi : \mathbb{R}^{n_x} \times \mathbb{R}^m \times \mathbb{R}^{n_p} \times \mathbb{R} \rightarrow \mathbb{R}^{n_x}$, which depends on f , such that

$$\tilde{x}(t_{n+1}) = G(\tilde{x}(t_n), \tilde{y}_m^n, \lambda)(h_n) = \Phi(\tilde{x}(t_n), \tilde{y}_m^n, \lambda, h_n),$$

for any $t_n \in \mathcal{P}$ and $h_n \in (0, h]$.

We are now ready to provide an estimate for the cumulative error between $\hat{x}(t_n)$ and $\tilde{x}(t_n)$.

Lemma 4.3. Assume Φ is Lipschitz with respect to the first argument and with Lipschitz constant $L_\Phi > 0$. Suppose the residual DeepONet is well trained so that the neural network architecture satisfies (7). Then, we have

$$\|\hat{x}(t_n) - \tilde{x}(t_n)\| \leq \frac{1 - L_\Phi^n}{1 - L_\Phi} \epsilon.$$

Proof. Suppose Φ is Lipschitz and the residual DeepONet satisfies the universal approximation theorem of neural networks (7). Then, for any $t_n \in \mathcal{P}$ and $h_n \in (0, h]$, we have

$$\begin{aligned} \|\hat{x}(t_{n+1}) - \tilde{x}(t_{n+1})\| &= \|G_{\theta^*}^\epsilon(\hat{x}(t_n), \tilde{y}_m^n, \lambda) + G_{\text{approx}}(\hat{x}(t_n), \tilde{y}_m^n, \lambda)(h_n) - G(\tilde{x}(t_n), \tilde{y}_m^n, \lambda)(h_n)\| \\ &\leq \|G_{\theta^*}^\epsilon(\hat{x}(t_n), \tilde{y}_m^n, \lambda) + G_{\text{approx}}(\hat{x}(t_n), \tilde{y}_m^n, \lambda)(h_n) - G(\hat{x}(t_n), \tilde{y}_m^n, \lambda)(h_n)\| \\ &\quad + \|G(\hat{x}(t_n), \tilde{y}_m^n, \lambda)(h_n) - G(\tilde{x}(t_n), \tilde{y}_m^n, \lambda)(h_n)\| \\ &\leq \|G_{\theta^*}^\epsilon(\hat{x}(t_n), \tilde{y}_m^n, \lambda) - \varphi(\hat{x}(t_n), \tilde{y}_m^n, \lambda)\| \\ &\quad + \|\Phi(\hat{x}(t_n), \tilde{y}_m^n, \lambda, h_n) - \Phi(\tilde{x}(t_n), \tilde{y}_m^n, \lambda, h_n)\| \\ &\leq \epsilon + L_\Phi \|\hat{x}(t_n) - \tilde{x}(t_n)\|. \end{aligned}$$

The Lemma follows then from $\hat{x}(t_0) = \tilde{x}(t_0) = x_0$. \square

The following theorem provides the final estimate for the cumulative error between $x(t_n)$ obtained using the *true* solution operator G and $\hat{x}(t_n)$ obtained using the proposed residual DeepONet numerical scheme (see Algorithm 2).

Theorem 4.4. For any $t_n \in \mathcal{P}$ and $h_n \in (0, h]$, we have

$$\|x(t_n) - \hat{x}(t_n)\| \leq \frac{1 - r^n}{1 - r} \mathcal{E} + \frac{1 - L_\Phi^n}{1 - L_\Phi} \epsilon.$$

We conclude from the above theorem that the error accumulates due to (i) the input approximation and (ii) the neural network approximation error. Thus, even if the proposed residual DeepONet generalizes effectively, the final approximation may be inaccurate due to an inadequate input approximation. However, we will show empirically in the next section that for reasonable values of h , the proposed DeepONet framework effectively approximates the dynamic response of power grid devices even in the extreme case when we locally approximate y using *one* sensor, *i.e.*, $m = 1$.

5 The Data Aggregation (Dagger) Algorithm

This section considers the problem of a DeepONet-based generator interacting with a simulator. In such a problem, a significant concern is the error propagation and accumulation of Algorithms 1 and 2 when interacting with the numerical simulator. Moreover, this error accumulation drastically increases in the small training data regime.

This small data regime may occur, for example, when we (i) partially know the state-input space, *i.e.*, we only know $\hat{\mathcal{X}} \times \hat{\mathcal{Y}} \subset \mathcal{X} \times \mathcal{Y}$ or (ii) use an expensive large-scale power grid simulator to solve for the interacting variables $y(t_n)$. Note that the small data regime is likely the scenario we will have if we include the control inputs and the generator parameters. In particular, sampling from the product space $\mathcal{X} \times \mathcal{Y} \times \mathcal{U} \times \Lambda$ may be prohibitively expensive.

Training a DeepONet-based generator (data-driven or residual) in the small data regime may compromise generalization. Furthermore, using Algorithms 1 or 2 with DeepONets that fail to generalize effectively may lead to error propagation and accumulation. This error accumulation will make the data-driven and residual DeepONet experience distributional drift. That is, the DeepONets will observe inputs $\{x(t_n), y(t_n)\}$ not included in the original training dataset. Observing such inputs leads to more error propagation and accumulation, jeopardizing the long-term prediction accuracy of Algorithms 1 and 2.

To handle this distributional drift, we draw inspiration from the behavioral cloning literature [40] and propose a data aggregation (Dagger) strategy, detailed in Algorithm 3, that trains and fine-tunes data-driven or residual DeepONets. Dagger is an iterative algorithm that proceeds as follows. In the first iteration, we train the data-driven (resp. residual) DeepONet G_θ (resp. G_θ^ϵ) using the training dataset $\mathcal{D}_{\text{train}}$. Then, we rollout (for n_{rollout} times) Algorithm 1 (resp. Algorithm 2) with the trained DeepONet G_{θ^*} (resp. $G_{\theta^*}^\epsilon$) to collect a new dataset of inputs $\mathcal{D} = \{x_k(t_n), y_k(t_n)\}_{k \geq 1}$ generated from the interaction with the simulator. We then use the true solution operator \tilde{G} to label the new dataset \mathcal{D} . Finally, we aggregate the datasets as follows $\mathcal{D}_{\text{train}} = \mathcal{D}_{\text{train}} \cup \mathcal{D}$. We repeat this procedure for n_{iter} iterations.

Note that the main idea behind this Dagger Algorithm 3 is to build up the set of inputs that the trained DeepONet is likely to encounter when interacting with the simulator. Collecting such a set of inputs will reduce distributional drift and error accumulation.

6 Numerical Experiments

We test the proposed DeepONet frameworks using experiments on the two-axis (transient) generator model [41] that interacts with a power grid modeled as an infinite bus (see Figure 3). In these experiments, we (i) compare the supervised training efficacy and efficiency for the DeepONet and residual DeepONet frameworks (Section 6.4); (ii) analyze the sensitivity of the proposed models using different input distributions and dataset sizes (Section 6.5); and (iii) verify the Dagger algorithm’s performance for different initial conditions and fault sequences (Sec-

Algorithm 3: The Data Aggregation (DAgger) Algorithm

- 1 **Require:** Initial training dataset $\mathcal{D}_{\text{train}} = \{x_k(t_n), y_k(t_n), h_k, G_{*,k}\}_{k=1}^{N_{\text{train}}}$, number of rollouts n_{rollout} , true solution operator \tilde{G} , and time partition $\mathcal{P} \subset [0, T_{\text{DAgger}}]$ (s).
 - 2 **for** $n = 1, \dots, n_{\text{iter}}$ **do**
 - 3 train the DeepONet G_θ using the dataset $\mathcal{D}_{\text{train}}$
 - 4 run Algorithm 1 or 2 for n_{rollout} times using the trained DeepONet G_{θ^*} and partition \mathcal{P}
 - 5 collect the dataset of inputs $\mathcal{D} = \{x_k(t_n), y_k(t_n)\}_{k \geq 1}$ visited by G_{θ^*}
 - 6 use G to label the dataset of inputs \mathcal{D}
 - 7 aggregate the datasets: $\mathcal{D}_{\text{train}} = \mathcal{D}_{\text{train}} \cup \mathcal{D}$
 - 8 **end**
 - 9 **Return:** trained DeepONet G_{θ^*} .
-

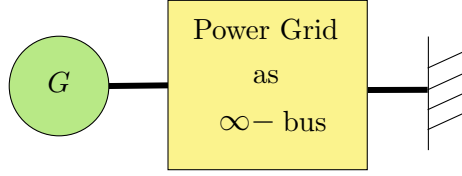


Figure 3: A synchronous (transient) generator model G that interacts with the rest of the power grid modeled as an infinite (∞) bus.

tion 6.6). For all the experiments, the predictions of the proposed DeepONet models are used to solve the network equations of the infinite bus. In addition, Appendix A provides an experiment that uses DeepONet to shadow the response of a transient generator model interacting with a two-area power grid model. We simulate this power grid model using the Power System Toolbox [10]—a Matlab-based power grid transient simulation engine. Note that for this experiment in Appendix A, the predictions are not used to solve the power flow and network equations. Let us start this section by describing this experiment’s power grid model, the data generation process, the neural networks, and the training protocol.

6.1 The Power Grid Model

The non-autonomous system that describes the two-axis (transient) generator model interacting with an infinite bus is given by [41]:

$$\begin{aligned}
 T'_{d_o} \frac{dE'_q}{dt} &= -E'_q - (X_d - X'_d)I_d + E_{fld} \\
 T'_{q_o} \frac{dE'_d}{dt} &= -E'_d + (X_q - X'_q)I_q \\
 \frac{d\delta}{dt} &= \omega - \omega_s \\
 \frac{2H}{\omega_s} \frac{d\omega}{dt} &= T_M - T_E - D(\omega - \omega_s)
 \end{aligned} \tag{8}$$

where

$$T_E = E'_d I_d + E'_q I_q + (X'_q - X'_d) I_d I_q.$$

In the above, the vector of states is $x(t) = (E'_q(t), E'_d(t), \delta(t), \omega(t))^\top$, the set of parameters are $\{T'_{d_o}, X_d, X'_d, E_{fld}, T'_{q_o}, X_q, X'_q, \omega_s, H, T_M, D\}$ (note that the outputs of the exciter E_{fld} and the turbine governor T_M are constant in this experiment. Enabling them as inputs to the generator

model is straightforward), and the vector of inputs is $y(t) = (I_d, I_q)^\top$, which one obtains by solving the network equations of the infinite bus:

$$\begin{aligned} 0 &= (R_s + R_e)I_d - (X'_q + X_{ep})I_q - E'_d + V_\infty \sin(\delta - \theta_\infty) \\ 0 &= (R_s + R_e)I_q + (X'_d + X_{ep})I_d - E'_q + V_\infty \sin(\delta - \theta_\infty), \end{aligned} \quad (9)$$

where $\{R_s, R_e, X_{ep}\}$ are parameters and $V_\infty \angle \theta_\infty$ the voltage phasor of the infinite bus. Observe that the network equations (9) depend on the predicted state variables $\delta(t)$, $E'_d(t)$, and $E'_q(t)$. Thus, any DeepONet prediction errors will impact the solution of (9).

6.2 Data Generation

Training data. To generate the training dataset $\mathcal{D}_{\text{train}}$ for the proposed DeepONet frameworks, we discretize and simulate (using Runge-Kutta 4 [18]) the above non-autonomous model (8)-(9). $\mathcal{D}_{\text{train}}$ consists of N_{train} samples of the form:

$$\{x(t_n), y(t_n), h, G_*(x(t_n), y(t_n))(h)\}.$$

To obtain the input to the Branch Net, *i.e.*, $(x(t_n), y(t_n))$, one can use one of the following two procedures. The first procedure uniformly samples from the *state-input* distribution. That is, we sample $x(t_n)$ from the state space $\mathcal{X} := \{x : \delta \in [-\pi, 4\pi], \omega \in [0.0, \pi/2], E'_d \in [-1.0, 1.0], E'_q \in [0.0, 1.5]\}$ and $y(t_n)$ from the input space $\mathcal{Y} := \{y : I_d \in [-1.0, 3.0], I_q \in [-1.0, 1.0]\}$. The second procedure uniformly samples $x(t_n)$ from the state space \mathcal{X} . Then, using the sampled $x(t_n)$, we solve the *network equations* (9) for $y(t_n)$.

To obtain the input to the Trunk Net, we uniformly sample h from the interval $[0.0, 0.25]$ (seconds). Finally, we obtain the DeepONet's output G_* as follows. For the incremental operator G_Δ , one first obtains $x(t_n + h)$ by discretizing and simulating the non-autonomous dynamics (8) with the sampled values of $x(t_n)$, $y(t_n)$, and h . Then, the incremental operator is given by $G_\Delta = x(t_n + h) - x(t_n)$. On the other hand, to compute the residual operator G_ϵ , we proceed as follows. First, we obtain the approximate prediction by computing the solution operator of the approximate model, *i.e.*, $G_{\text{approx}} \equiv x_{\text{approx}}(t_n + h)$ using $x(t_n)$, $y(t_n)$, and h . The approximate model in this experiment corresponds to the same non-autonomous dynamics (8) except for the angular velocity equation, which reads as follows:

$$\frac{2H}{\omega_s} \frac{d\omega}{dt} = T_M - T_E - \beta D(\omega - \omega_s)$$

In the above, we use the parameter $\beta = 0.5$ to change the model's fidelity. Using the approximate and true solution operators, we compute the residual operator via $G_\epsilon \equiv G - G_{\text{approx}} = x(t_n + h) - x_{\text{approx}}(t_n + h)$.

Test data. We generate two test datasets of $N_{\text{test}} = 500$ solution trajectories $\{x^{(i)}(t) : t \in \mathcal{P}\}_{i=1}^{N_{\text{test}}}$ for a given time partition \mathcal{P} . The *first* test dataset is obtained as follows. Let $x^* = (\delta^*, \omega^*, E'_d, E'_q)^\top$ denote the equilibrium point of (8). Then, one obtains each test trajectory from an initial condition $x_o \in \mathcal{X}_o := \{x : \delta = \delta^*, \omega = \gamma\omega^*, E'_d = E'_d, E'_q = E'_q\}$, where γ is uniformly sampled from the interval $[0.2, 1.5]$.

On the other hand, each trajectory of the *second* test dataset starts from the equilibrium point $x_o = x^*$. Then, at time $t_f = 1.0$ seconds, we simulate a fault/disturbance by changing the impedance of the infinite bus. At the time $t_f + \Delta t_f$, we clear the fault by recovering the original value of the impedance. Each trajectory has a different fault duration Δt_f , which we uniformly sample from the interval $[0.05, 1.0]$.

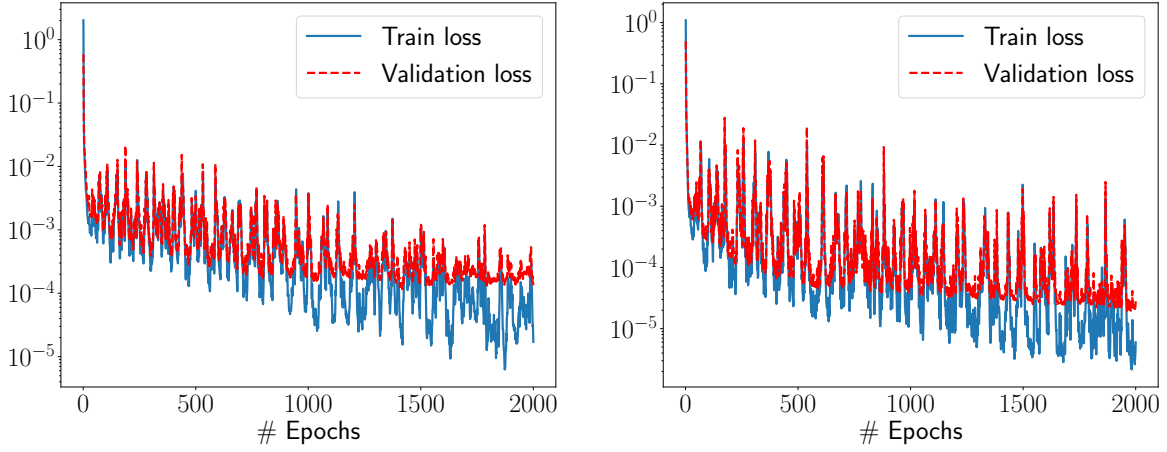


Figure 4: Comparison of the training and validation loss between (*left*) data-driven DeepONet and (*right*) residual DeepONet.

6.3 Neural Nets and Training Protocol

Neural Nets. We implemented the proposed frameworks using PyTorch [35]¹. To build the Branch and Trunk Nets, we (i) used the modified fully-connected network architecture proposed in [47] and implemented in our previous work [30, 32], (ii) employed leaky ReLU activation functions, and (iii) performed a simple hyper-parameter optimization routine to find the best architectures.

Training. We trained the parameters of the neural networks using traditional supervised learning and the proposed data aggregation algorithm (see Section 5). In particular, we optimized the DeepONet parameters using Adam [22] with default parameters and a learning rate of $\eta = 5 \times 10^{-3}$. We also implemented a scheduler that reduces this learning rate whenever the training reaches a plateau. Finally, we normalized the inputs and outputs during training and testing.

6.4 Experiment 1. Supervised Training

This first experiment evaluates the supervised training efficacy and efficiency of the data-driven and the residual DeepONets. To this end, we trained the proposed frameworks using $N_{\text{train}} = 2000$ samples (80% training and 20% validation). In particular, the inputs to the Branch Net were obtained by sampling the state-input distribution $\mathcal{X} \times \mathcal{Y}$. We ran supervised training for $N_{\text{epochs}} = 2000$ epochs and validated the frameworks after each epoch. Figure 4 illustrates the convergence of the training and validation losses. They depict that the convergence to adequate training and validation loss values ($\sim 10^{-5}$ for data-driven and $\sim 10^{-6}$ for residual) is faster for the residual DeepONet. Such a result shows that including prior information (*e.g.*, the physics of the underlying problem) can improve the training process.

Using the trained DeepONet frameworks, we tested how well they generalize outside the training dataset. To this end, we first selected random trajectories from the test dataset and compared the proposed DeepONet predictions against the ground truth. Figure 5 and Figure 6 depict the predicted state trajectories and network response when employing the data-driven DeepONet over a uniform partition $\mathcal{P} \subset [0, 10]$ (s) of step size $h = 0.05$. Similarly, Figure 7 and Figure 8 illustrate the predicted state trajectories and the network trajectories for the residual DeepONet over an irregular partition $\mathcal{P} \subset [0, 10]$ (s) of 200 random distinct points. Observe that the

¹We will make the code available after publication

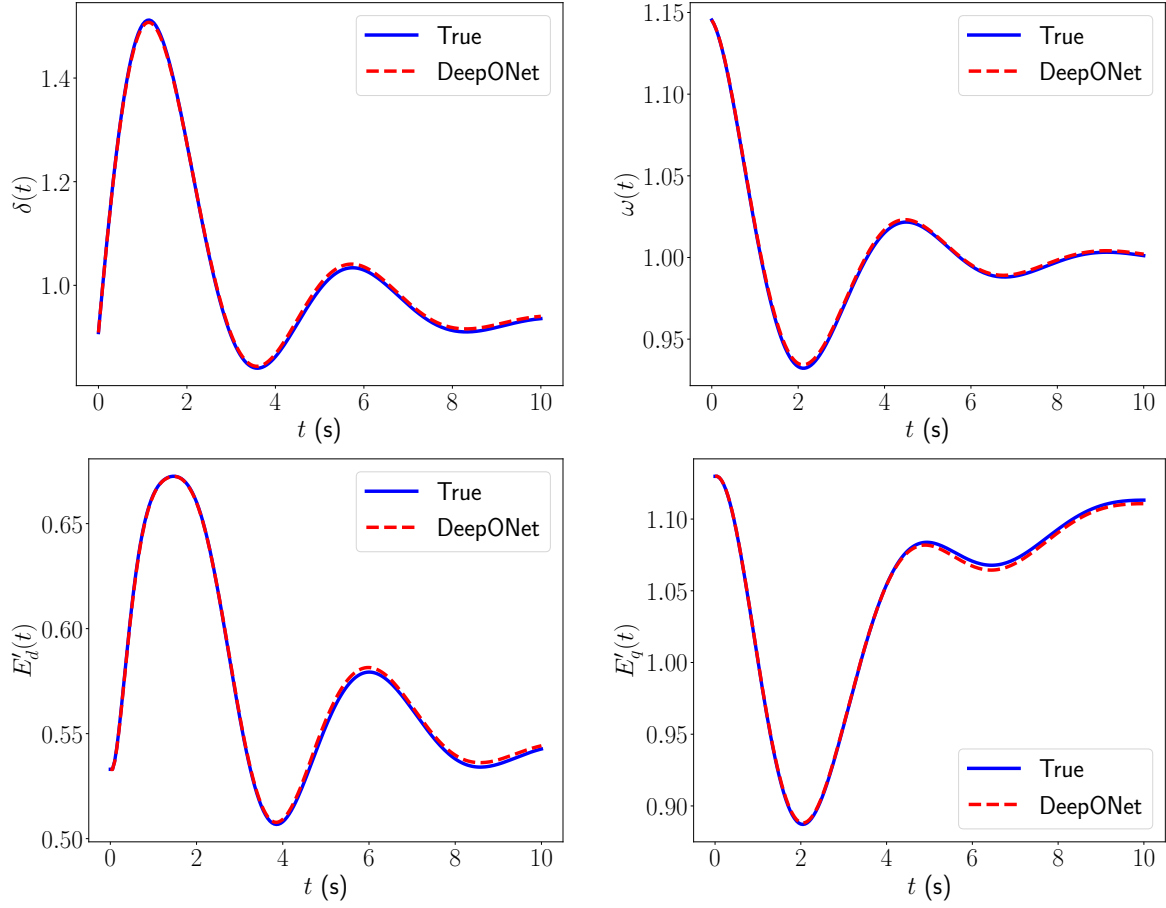


Figure 5: Comparison of the data-driven DeepONet prediction with the true trajectory of the synchronous generator state $x(t) = (\delta(t), \omega(t), E'_d(t), E'_q(t))^T$ within the uniform partition $\mathcal{P} \subset [0, 10]$ (s) of constant step size $h = 0.05$.

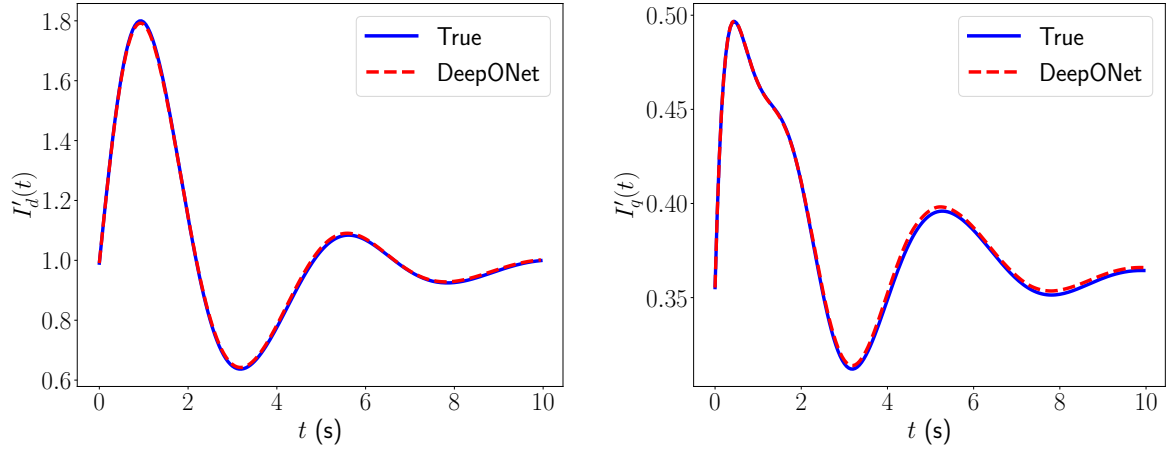


Figure 6: Comparison of the resulting network input $y(t) = (I'_d(t), I'_q(t))^T$ for the data-driven DeepONet trained within the uniform partition $\mathcal{P} \subset [0, 10]$ (s) of constant step size $h = 0.05$.

proposed DeepONet frameworks (i) accurately predict the state trajectories and (ii) do not introduce and propagate errors when solving for the network equations (9). Furthermore, note that the proposed residual DeepONet can accurately learn unstable and oscillatory trajectories, which is often challenging.

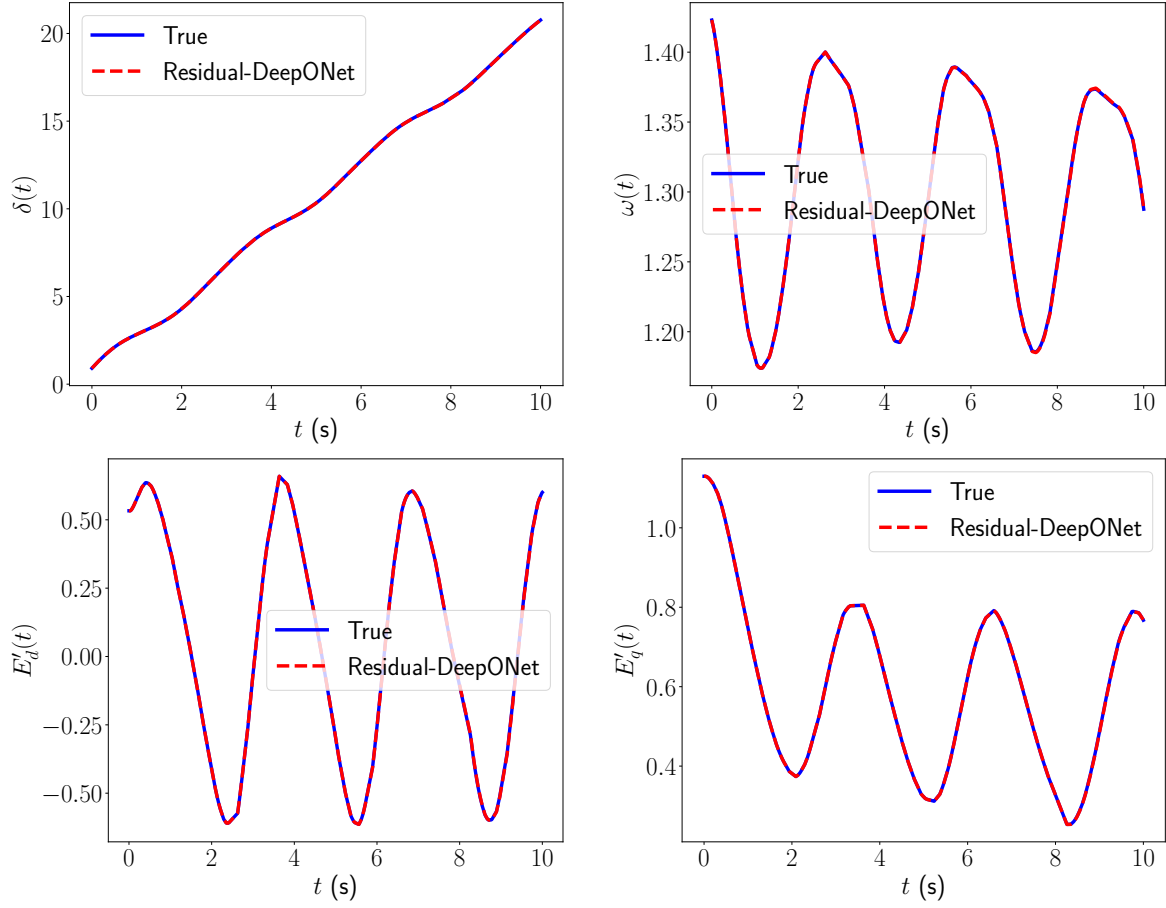


Figure 7: Comparison of the residual DeepONet prediction with the true trajectory of the synchronous generator state $x(t) = (\delta(t), \omega(t), E_d'(t), E_q'(t))^T$ within the irregular partition $\mathcal{P} \subset [0, 10]$ (s) of size 200 (distinct random points).

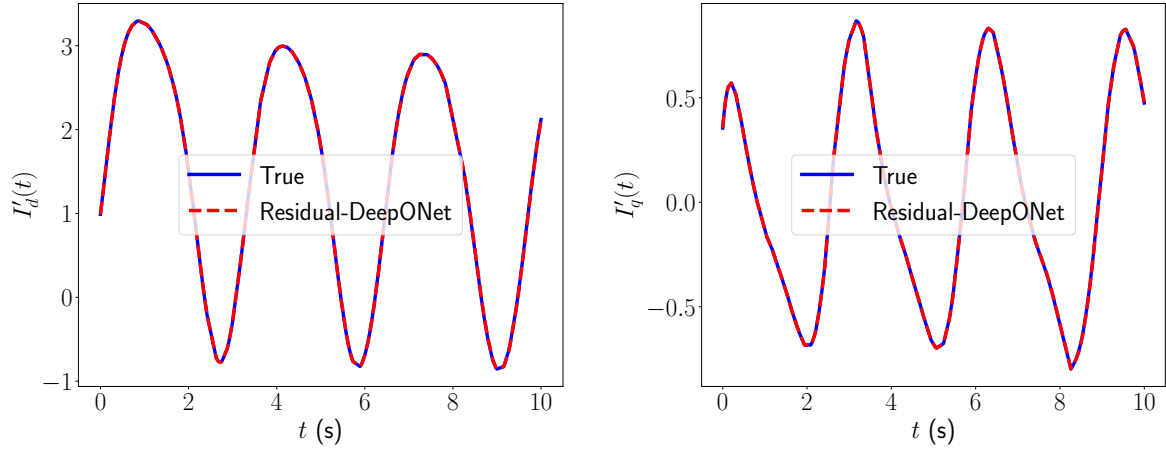


Figure 8: Comparison of the resulting network input $y(t) = (I_d'(t), I_q'(t))^T$ for the residual DeepONet trained within the irregular partition $\mathcal{P} \subset [0, 10]$ (s) of size 200 (distinct random points).

To further study the proposed frameworks' predictive and generalization capabilities, we computed the mean and standard deviation (st. dev.) of the L_2 -relative error (between the predicted state and network trajectories and ground truth) for all 500 test trajectories. Table 1 (resp. Table 2) illustrate the results for the data-driven (resp. residual) DeepONet. Also, we

	$\delta(t)$	$\omega(t)$	$E'_d(t)$	$E'_q(t)$	$I'_d(t)$	$I'_q(t)$
mean L_2 %	1.284 %	0.315 %	2.901 %	1.181 %	2.184 %	3.488 %
st.dev. L_2 %	3.455 %	0.768 %	8.564 %	3.614 %	5.054 %	10.340 %

Table 1: The mean and standard deviation (st.dev.) of the L_2 -relative error between the predicted (data-driven DeepONet) and the actual response of the (i) synchronous generator state and (ii) network’s input for 500 initial conditions sampled from the set \mathcal{X}_o and within the uniform partition $\mathcal{P} \subset [0, 10]$ (s) of constant step size $h = 0.05$.

	$\delta(t)$	$\omega(t)$	$E'_d(t)$	$E'_q(t)$	$I'_d(t)$	$I'_q(t)$
mean L_2 %	0.209 %	0.052 %	0.580 %	0.221 %	0.443 %	0.698 %
st.dev. L_2 %	0.519 %	0.126 %	1.584 %	0.593 %	1.068 %	2.054 %

Table 2: The mean and standard deviation (st.dev.) of the L_2 -relative error between the predicted (residual DeepONet) and the actual response of the (i) synchronous generator state and (ii) network’s input for 500 initial conditions sampled from the set \mathcal{X}_o and within the irregular partition $\mathcal{P} \subset [0, 10]$ (s) of size 200 (distinct random points).

compared our results with results from a trained, fully-connected neural network (FNN). Note that FNNs have often been employed in model-based reinforcement learning [48] to learn a surrogate of the environment, which can predict the next state using the current state and the action. Thus, naturally, we can adopt the same idea and use FNNs to predict the response of synchronous generators. Table 3 shows the mean and standard deviation of the L_2 -relative errors between the FNN prediction and ground truth for all test trajectories.

The results show the following. (i) FNN fails to predict the dynamic response of the generator and accumulates errors over time. In practice, the reinforcement learning community reduces this error accumulation by employing ensembles and uncertainty quantification [11]. Such solutions, however, increase the computational inference cost. (ii) In contrast to FNN, the proposed frameworks can control the error accumulation without increasing the computational cost. Our data-driven DeepONet, for example, keeps the mean L_2 error for all states below 5%. We will show in the following experiments that the L_2 error can be reduced further by increasing the number of training samples or using the DAgger algorithm. (iii) Finally, we obtained the best results from the residual DeepONet. Residual DeepONet always keeps the mean L_2 error below 1%. Such a result shows that incorporating prior information (*e.g.*, the underlying physics of the problem) enhances generalization by constraining the space of possible learning responses even with limited training examples.

6.5 Experiment 2. Sensitivity

This experiment first analyzes the proposed methods’ generalization capabilities when the training inputs $(x(t_n), y(t_n))$ to the Branch Net are obtained by sampling $x(t_n)$ from \mathcal{X} and solving the network equations (9) for $y(t_n)$. To this end, we trained the proposed DeepONets as in Experiment 1 and computed the L_2 -relative errors for all 500 test trajectories. Table 4 (resp. Table 5) depicts the results for the data-driven (resp. residual) DeepONet. These results illustrate that training using inputs obtained by solving (9) reaches similar L_2 errors as when training using inputs sampled from the input space \mathcal{Y} . We remark, however, that training using the (i) state-input distribution requires knowing the spaces \mathcal{X} and \mathcal{Y} and (ii) network equations requires solving the whole power grid dynamics, which may be expensive for large-scale models.

We now study how the mean L_2 -relative errors for all the 500 test trajectories vary accord-

	$\delta(t)$	$\omega(t)$	$E'_d(t)$	$E'_q(t)$	$I'_d(t)$	$I'_q(t)$
mean L_2 %	22.515 %	4.026 %	37.820 %	15.309 %	25.795 %	36.496 %
st.dev. L_2 %	16.281 %	4.729 %	46.873 %	13.638 %	23.933 %	45.923 %

Table 3: The mean and standard deviation (st.dev.) of the L_2 -relative error between the predicted (feed-forward neural network) and the actual response of the (i) synchronous generator state and (ii) network’s input for 500 initial conditions sampled from the set \mathcal{X}_o and within a uniform partition $\mathcal{P} \subset [0, 10]$ (s) of constant step size $h = 0.05$.

	$\delta(t)$	$\omega(t)$	$E'_d(t)$	$E'_q(t)$	$I'_d(t)$	$I'_q(t)$
mean L_2 %	1.955 %	0.410 %	4.942 %	1.734 %	3.696 %	5.294 %
st.dev. L_2 %	2.908 %	0.663 %	8.422 %	2.597 %	5.251 %	10.159 %

Table 4: The mean and standard deviation (st.dev.) of the L_2 -relative error between the predicted (data-driven DeepONet trained using the network equations (9)) and the actual response of the (i) synchronous generator state and (ii) network’s input for 500 initial conditions sampled from the set \mathcal{X}_o and within the uniform partition $\mathcal{P} \subset [0, 10]$ (s) of constant step size $h = 0.05$.

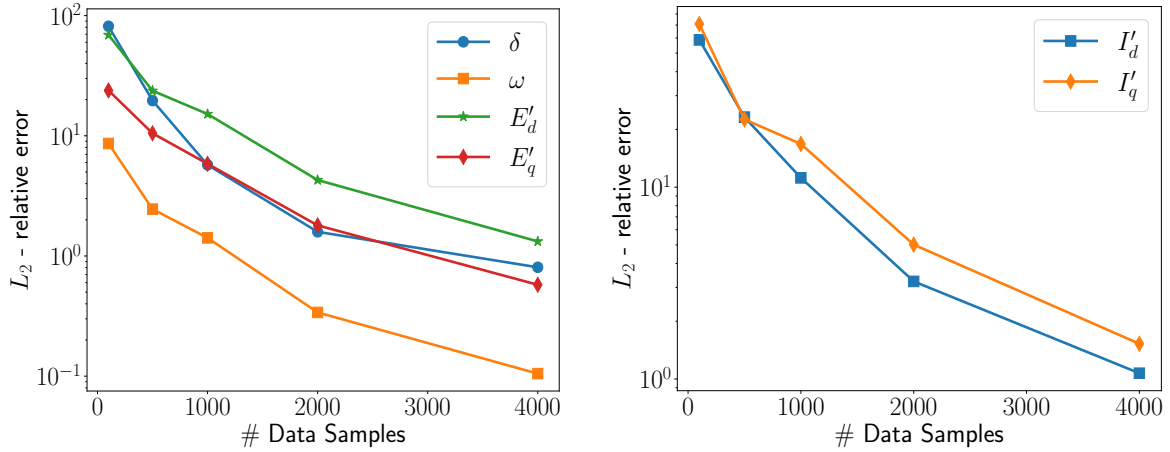


Figure 9: The mean L_2 -relative error % of 500 predicted trajectories with data-driven DeePONet as a function of the number of training samples for the (left) generator states $x(t) = (\delta(t), \omega(t), E'_d(t), E'_q(t))^T$ and (right) network inputs $y(t) = (I'_d(t), I'_q(t))^T$.

ing to the number of training data samples. We let the data samples vary within the set $\{100, 500, 1000, 2000, 4000\}$ for simplicity. Figure 9 (resp. Figure 10) illustrates how the mean L_2 -relative errors (for the state and network trajectories) vary as we increase the number of training data samples for the data-driven (resp. residual) DeepONet. The results illustrate that if we increase the number of training data samples, the L_2 -relative errors and the error accumulation will decrease. We also observe that regardless of the training dataset size, the residual DeepONet (*i.e.*, using prior information) always leads to better generalization and decreased error accumulation.

6.6 Experiment 3. The DAgger Algorithm

We now use the data aggregation (DAgger) algorithm (see Section 5 for details) to train the residual DeepONet framework. Training the data-driven DeepONet with DAgger leads to similar results. As described in Section 5, we advocate for DAgger when sampling the state-input space $\mathcal{X} \times \mathcal{Y}$ may become prohibitively expensive, and hence, supervised learning may lead to

	$\delta(t)$	$\omega(t)$	$E'_d(t)$	$E'_q(t)$	$I'_d(t)$	$I'_q(t)$
mean L_2 %	0.275 %	0.062 %	0.762 %	0.303 %	0.558 %	0.910 %
st.dev. L_2 %	0.676 %	0.166 %	2.035 %	0.766 %	1.379 %	2.655 %

Table 5: The mean and standard deviation (st.dev.) of the L_2 -relative error between the predicted (residual DeepONet trained using the network equations (9)) and the actual response of the (i) synchronous generator state and (ii) network’s input for 500 initial conditions sampled from the set \mathcal{X}_o and within the uniform partition $\mathcal{P} \subset [0, 10]$ (s) of constant step size $h = 0.05$.

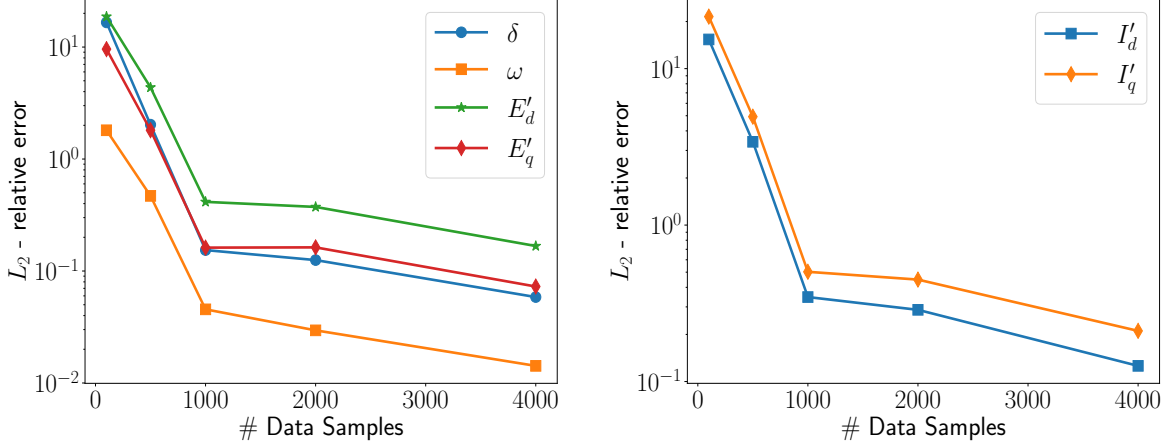


Figure 10: The mean L_2 -relative error % of 500 predicted trajectories with residual DeepONet as a function of the number of training samples for the (left) generator states $x(t) = (\delta(t), \omega(t), E'_d(t), E'_q(t))^T$ and (right) network inputs $y(t) = (I'_d(t), I'_q(t))^T$.

accumulation and propagation of errors. To simulate such a scenario, we assumed one could only collect $N_{\text{train}} = 100$ data samples for supervised learning. Then, we adopted $n_{\text{iters}} = 5$ iterations of the DAgger algorithm. Each iteration of DAgger predicted 10 rollouts sampled from distinct initial conditions $x(0) \in \mathcal{X}_o$ and over a uniform partition $\mathcal{P} \subset [0.0, 5.0]$ (s) of step size $h = 0.05$. After training with DAgger, we tested the generalization capability of the residual DeepONet using the test dataset of 500 disturbance trajectories. This test scenario is challenging because DAgger never observed a disturbance trajectory during training.

We first selected a random disturbance trajectory from the test dataset and compared the proposed residual DeepONet’s predictions against the ground truth. Figure 11 and Figure 12 illustrate the residual DeepONet’s predicted state trajectories and the network response. We observe again that the proposed residual DeepONet (i) accurately predicts the state trajectories and (ii) does not introduce and propagate errors when solving for the network equations (9) with disturbance.

To further study the generalization for the residual DeepONet trained with the DAgger algorithm, we computed the mean and standard deviation (st. dev.) of the L_2 -relative error (for the predicted state and network trajectories) for all 500 test disturbance trajectories. Table 6 shows the results for the residual DeepONet trained with DAgger. These results illustrate that the residual DeepONet keeps the mean L_2 -relative error below 0.01 % for all state and network trajectories. Such a result implies that residual DeepONet propagates almost no errors to the network equations (9).

To conclude this experiment, we study how the mean L_2 -relative errors for all the 500 test disturbance trajectories vary as a function of the number of DAgger iterations. In particular, we assumed the DAgger iterations used to train the residual DeepONet vary within the set

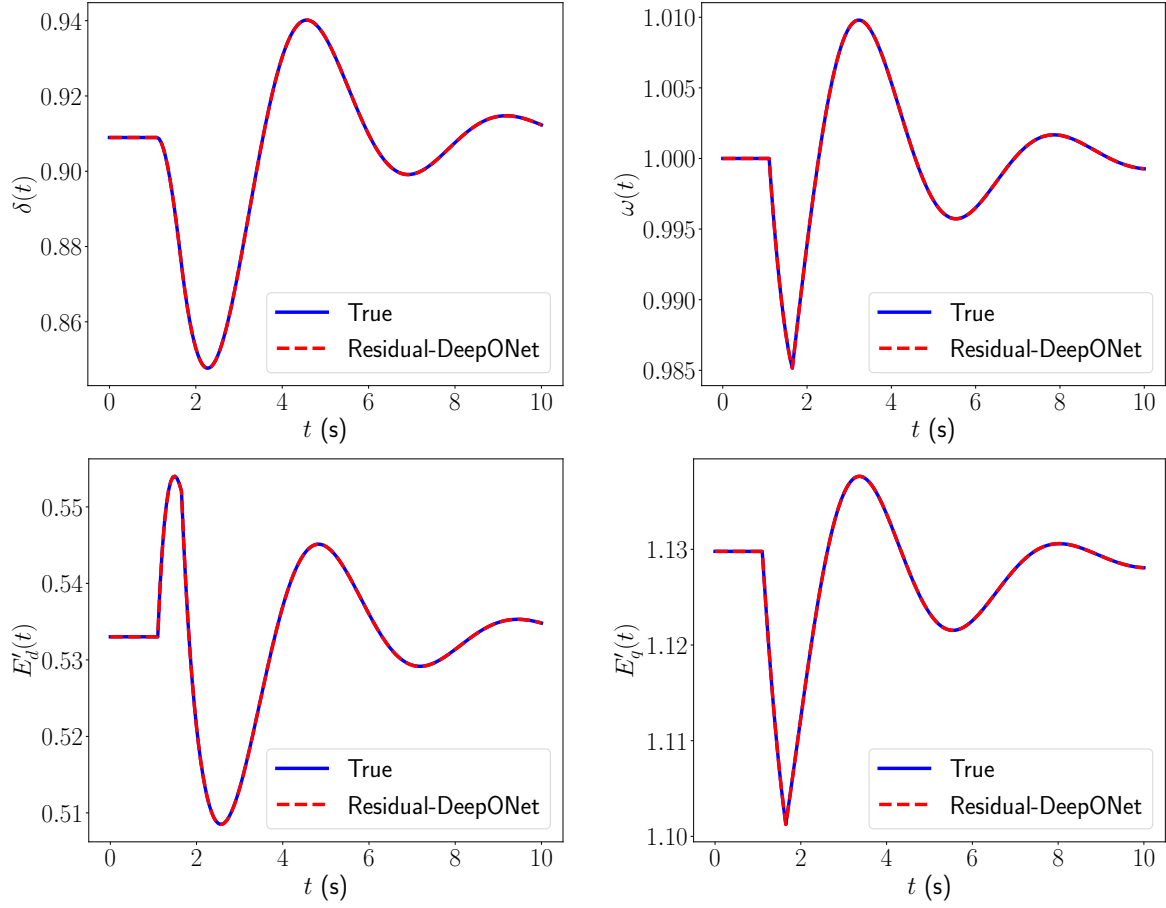


Figure 11: Comparison of the residual DeepONet prediction with the true fault trajectory of the synchronous generator state $x(t) = (\delta(t), \omega(t), E'_d(t), E'_q(t))^\top$ within the irregular partition $\mathcal{P} \subset [0, 10]$ (s) of size 200.

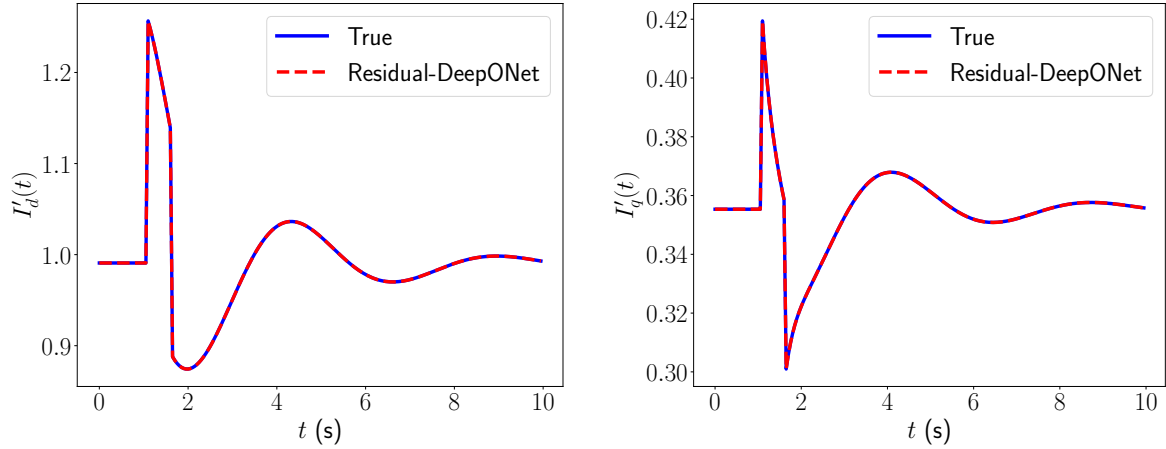


Figure 12: Comparison of the resulting network input $y(t) = (I'_d(t), I'_q(t))^\top$ after a random disturbance for the residual DeepONet trained within the irregular partition $\mathcal{P} \subset [0, 10]$ (s) of size 200.

$\{1, 2, 3, 4, 5\}$. Figure 13 shows how the mean L_2 -relative errors (for the state and network trajectories) vary as we increase the number of DAGger iterations for the residual DeepONet. These results illustrate that the L_2 -relative errors and the error accumulation decrease as we increase the number of DAGger iterations. This is because the DAGger algorithm aggregates

	$\delta(t)$	$\omega(t)$	$E'_d(t)$	$E'_q(t)$	$I'_d(t)$	$I'_q(t)$
mean L_2 %	0.0077 %	0.0007 %	0.0054 %	0.0032 %	0.0043 %	0.0058 %
st.dev. L_2 %	0.0004 %	0.0001 %	0.0003 %	0.0002 %	0.0001 %	0.0002 %

Table 6: The mean and standard deviation (st.dev.) of the L_2 -relative error between the residual DeepONet predicted and the actual response of the (i) synchronous generator state and (ii) network’s input for 500 different disturbance trajectories and within the uniform partition $\mathcal{P} \subset [0, 10]$ (s) of constant step size $h = 0.05$.

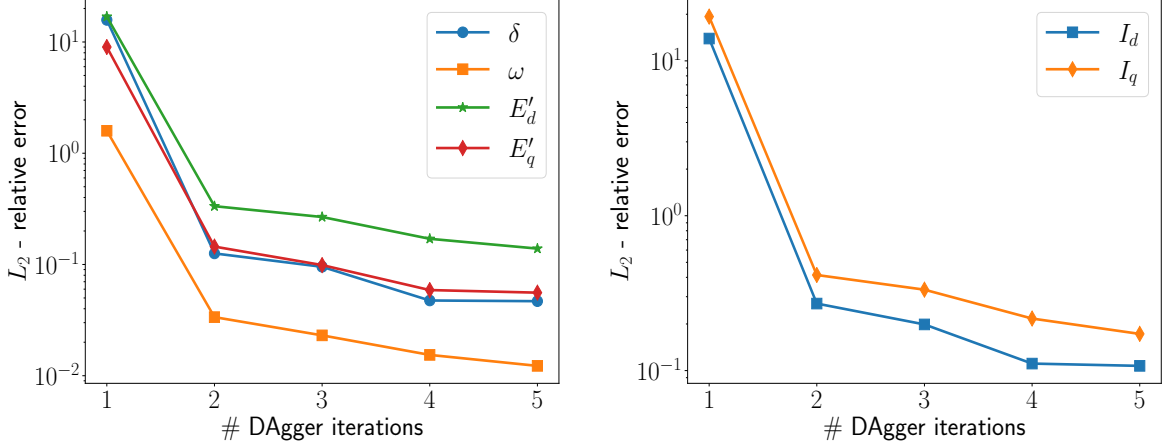


Figure 13: The mean L_2 -relative error % of 500 predicted trajectories with residual DeepONet as a function of the number of DAgger iterations (*left*) generator states $x(t) = (\delta(t), \omega(t), E'_d(t), E'_q(t))^T$ and (*right*) network inputs $y(t) = (I'_d(t), I'_q(t))^T$.

training data samples via the residual DeepONet is likely to encounter when interacting with the infinite bus model.

7 Discussion and Future Work

The experimental results presented in the previous section show the potential of the proposed DeepONet framework. In particular, our framework can effectively simulate/predict the dynamic response of power grid dynamic components interacting with a power grid. Let us now give a preamble of our future work.

On moving towards digital twins. We plan to develop a data assimilation method to calibrate the proposed DeepONet online. Such a method will enable shadowing the power grid *physical* component using a DeepONet-based *virtual* replica.

On securing the privacy of the power grid component’s owners. In this paper, we have assumed that we can freely collect training data from multiple owners (*e.g.*, generator or transmission owners). In practice, these owners may want to protect their privacy. Thus, building on our previous work [31], we plan in our future work to develop federated learning protocols for DeepONet training that secure proprietary mathematical models and data privacy.

On predicting large-scale power grids. We plan to develop the algorithmic and software workflows that will enable using the current DeepONet framework in a composable manner to build large-scale power grid simulators and digital twins. To this end, we will also develop DeepONet frameworks for reduced-order models, partially observable systems, and stochastic differential equations. Finally, we will use the composable large-scale model for optimizing, controlling, and

quantifying the uncertainty of smart grids with high penetration of renewable energy.

8 Conclusion

In this paper, we developed a Deep Operator Network (DeepONet) framework to learn the dynamic response of synchronous generators, which can interact with a simulator or the actual power grid. To this end, we designed our DeepONet to approximate the components' input/output solution operator for any arbitrary time interval. To simulate or predict the response for short/medium-term horizons, we introduced a DeepONet-based numerical scheme that can recursively use the trained framework. Furthermore, we developed a residual DeepONet framework that incorporates information from mathematical models. We also estimated the cumulative error of the corresponding residual DeepONet numerical scheme. For the case of a generator interacting with a numerical simulator for the rest of the grid, we designed a data aggregation (Dagger) algorithm for training and fine-tuning DeepONets using collected datasets with inputs that the trained DeepONet is likely to encounter when interacting with the simulator. Finally, we verified the efficacy of the proposed frameworks by learning a library of synchronous generators that interact with an infinite bus.

Appendix

A Shadowing a Transient Synchronous Generator

This experiment uses the proposed data-driven DeepONet to approximate the dynamic response of a synchronous generator using data collected with the Power System Toolbox (PST) [10]. In particular, the experiment focuses on the PST transient model of a generator with a default exciter connected to the two-area system depicted in Figure 14. Compared to the numerical experiments of Section 6, the trained DeepONet of this experiment only “shadows” the generator. That is, PST does not use the DeepONet’s predicted state $x(t_n + h)$ to solve the stator (2b) and network (2c) equations. As a result, the DeepONet always observes the correct interface inputs $y(t_n)$, simplifying the learning/inference task and alleviating the error accumulation. In addition, this scenario’s objective is also to represent the problem of learning the response of an actual synchronous generator connected to an actual power grid. Thus, we believe this is a first step towards building a generator digital twin, which we will study in our future work.

Training data. We generated the training data \mathcal{D}_{PST} by simulating $N_{\text{exp}} = 300$ experiments on PST. Each experiment proceeds as follows. (i) We simulated the two-area system on PST using a uniform partition $\mathcal{P} \subset [0.0, 5.0]$ (s), which starts at $t_0 = 0$ (s) and has a constant step size of $h = 0.05$. (ii) We simulated a fault at time $t_f = 0.1$ (s). (iii) Finally, we cleared the fault at time $t_f + \Delta t_f$, where Δt_f is the fault duration. We uniformly sampled this fault duration from the interval $[0.01, 0.1]$. After each experiment, we collected trajectory data, including the interacting input trajectories $\{y(t_n) : t_n \in \mathcal{P}\}$, where $y(t) = (I_d(t), I_q(t))^T$, the exciter input data $\{u(t_n) \equiv E_{\text{fd}}(t_n) : t_n \in \mathcal{P}\}$, and state trajectory data $\{x(t_n) : t_n \in \mathcal{P}\}$, where $x(t) = (\delta(t), \omega(t), E'_d(t), E'_q(t))^T$. We constructed our training dataset using this trajectory data. In particular, we used interpolation to discretize the inputs using $m = 2$ sensors, *i.e.*, $\tilde{y}_m^n := \{y(t_n + d_0), y(t_n + d_1)\}$ and $\tilde{u}_m^n := \{u(t_n + d_0), u(t_n + d_1)\}$, where $d_0 = 0.0$ and d_1 was uniformly sampled from the open interval $(0, h)$. Recall that in Section 6, we discretized the inputs using one sensor at time t_n . With these discretized inputs, we generated the final training dataset:

$$\mathcal{D}_{\text{PST}} = \{x_k(t_n), \tilde{y}_m^n 1, k, \tilde{u}_{m,k}^n, \{0, d_{m,k}\}, h_k, G_{\Delta,k}\}_{k=1}^{N_{\text{train}}}$$

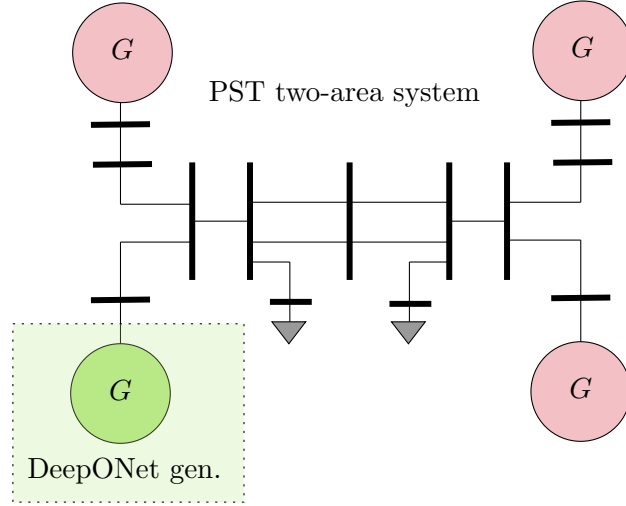


Figure 14: A synchronous (transient) generator model G that we approximate with a data-driven DeepONet. We trained the DeepONet using data collected from the two-area, four-generator system of the Power System Toolbox (PST).

Training protocol and test results. We trained the data-driven DeepONet using Adam [22]. We also designed a simple hyper-parameter optimization routine to find the optimal architectures for the Branch and Trunk nets. Then, we tested the data-driven DeepONet using a PST test trajectory not included in the training dataset. Figure 15 compares the predicted dynamic response of the proposed data-driven DeepONet with the ground truth. The results show excellent agreement between the predicted and actual response of the generator.

References

- [1] R. Anantharaman, A. Abdelrehim, F. Martinuzzi, S. Yalburgi, E. Saba, K. Fischer, G. Hertz, P. de Vos, C. Laughman, Y. Ma, et al. Composable and reusable neural surrogates to predict system response of causal model components. In *AAAI 2022 Workshop on AI for Design and Manufacturing (ADAM)*, 2021.
- [2] R. Anantharaman, Y. Ma, S. Gowda, C. Laughman, V. Shah, A. Edelman, and C. Rackauckas. Accelerating simulation of stiff nonlinear systems using continuous-time echo state networks. *arXiv preprint arXiv:2010.04004*, 2020.
- [3] P. Aristidou, D. Fabozzi, and T. Van Cutsem. Dynamic simulation of large-scale power systems using a parallel schur-complement-based decomposition method. *IEEE Transactions on Parallel and Distributed Systems*, 25(10):2561–2570, 2013.
- [4] G. W. Arnold. Challenges and opportunities in smart grid: A position article. *Proceedings of the IEEE*, 99(6):922–927, 2011.
- [5] T. Blochwitz, M. Otter, M. Arnold, C. Bausch, C. Clauß, H. Elmqvist, A. Junghanns, J. Mauss, M. Monteiro, T. Neidhold, et al. The functional mockup interface for tool independent exchange of simulation models. In *Proceedings of the 8th international Modelica conference*, pages 105–114. Linköping University Press, 2011.
- [6] S. L. Brunton, J. L. Proctor, and J. N. Kutz. Discovering governing equations from data by sparse identification of nonlinear dynamical systems. *Proceedings of the national academy of sciences*, 113(15):3932–3937, 2016.

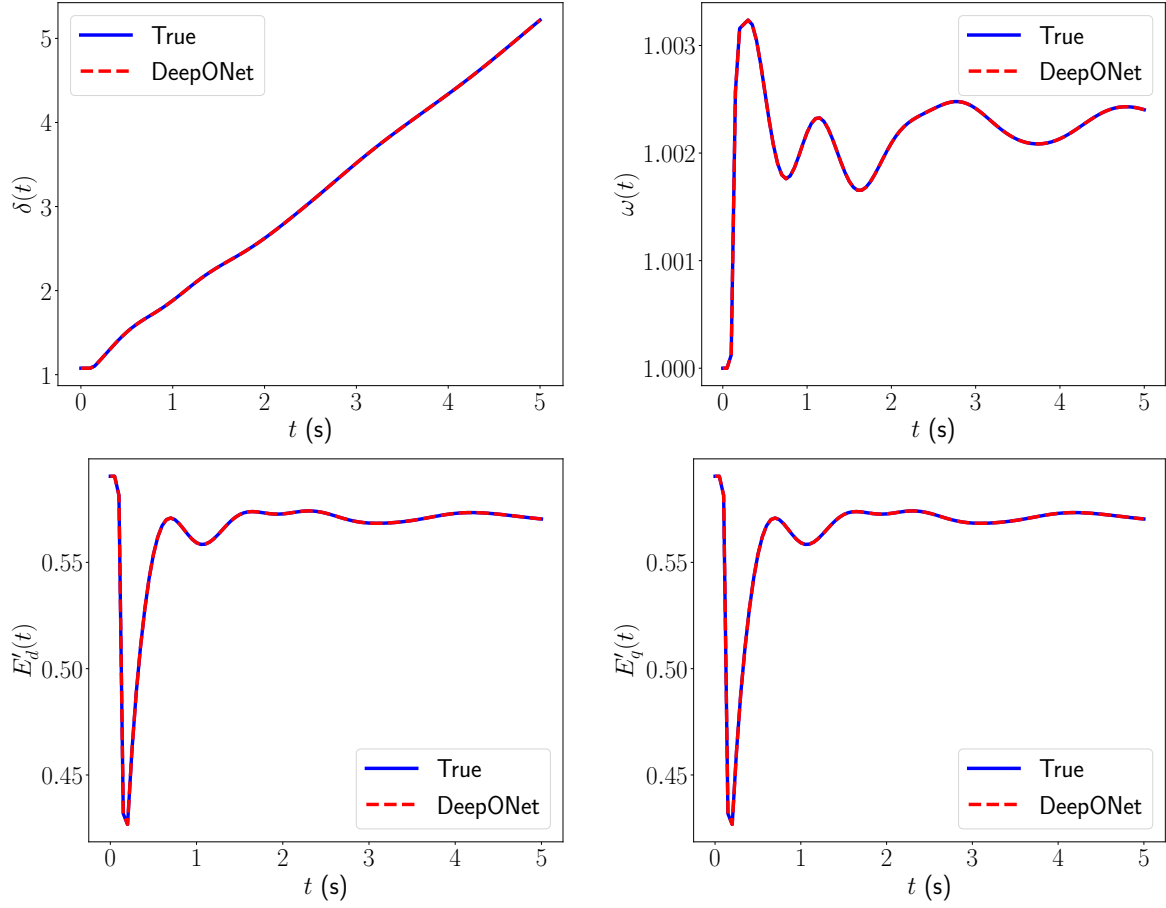


Figure 15: Comparison of the data-driven DeepONet prediction with the true fault test trajectory of the synchronous generator state $x(t) = (\delta(t), \omega(t), E'_d(t), E'_q(t))^T$. We simulated the test trajectory using the Power System Toolbox (PST) over the uniform partition $\mathcal{P} \subset [0, 5]$ (s) of constant step size $h = 0.05$.

- [7] S. L. Brunton, J. L. Proctor, and J. N. Kutz. Sparse identification of nonlinear dynamics with control (sindyc). *IFAC-PapersOnLine*, 49(18):710–715, 2016.
- [8] S. Cai, Z. Wang, L. Lu, T. A. Zaki, and G. E. Karniadakis. Deepm&mnet: Inferring the electroconvection multiphysics fields based on operator approximation by neural networks. *Journal of Computational Physics*, 436:110296, 2021.
- [9] T. Chen and H. Chen. Universal approximation to nonlinear operators by neural networks with arbitrary activation functions and its application to dynamical systems. *IEEE Transactions on Neural Networks*, 6(4):911–917, 1995.
- [10] J. H. Chow and K. W. Cheung. A toolbox for power system dynamics and control engineering education and research. *IEEE transactions on Power Systems*, 7(4):1559–1564, 1992.
- [11] K. Chua, R. Calandra, R. McAllister, and S. Levine. Deep reinforcement learning in a handful of trials using probabilistic dynamics models. *Advances in neural information processing systems*, 31, 2018.
- [12] M. Crow and M. Ilic. The parallel implementation of the waveform relaxation method for transient stability simulations. *IEEE Transactions on Power Systems*, 5(3):922–932, 1990.

- [13] G. Cybenko. Approximation by superpositions of a sigmoidal function. *Mathematics of control, signals and systems*, 2(4):303–314, 1989.
- [14] D. Fabozzi, A. S. Chieh, B. Haut, and T. Van Cutsem. Accelerated and localized newton schemes for faster dynamic simulation of large power systems. *IEEE Transactions on Power Systems*, 28(4):4936–4947, 2013.
- [15] A. J. Flueck. High-fidelity, faster than real-time dynamics simulation. In *2014 IEEE PES General Meeting— Conference & Exposition*, pages 1–1. IEEE, 2014.
- [16] G. Gurrula, A. Dimitrovski, S. Pannala, S. Simunovic, and M. Starke. Parareal in time for fast power system dynamic simulations. *IEEE Transactions on Power Systems*, 31(3):1820–1830, 2015.
- [17] R. Henriquez-Auba, J. D. Lara, D. S. Callaway, and C. Barrows. Transient simulations with a large penetration of converter-interfaced generation: scientific computing challenges and opportunities. *IEEE Electrification Magazine*, 9(2):72–82, 2021.
- [18] A. Iserles. *A first course in the numerical analysis of differential equations*. Number 44. Cambridge university press, 2009.
- [19] V. Jalili-Marandi and V. Dinavahi. Instantaneous relaxation-based real-time transient stability simulation. *IEEE Transactions on Power Systems*, 24(3):1327–1336, 2009.
- [20] G. E. Karniadakis, I. G. Kevrekidis, L. Lu, P. Perdikaris, S. Wang, and L. Yang. Physics-informed machine learning. *Nature Reviews Physics*, 3(6):422–440, 2021.
- [21] M. Kim, H. Yin, and G. Lin. Multi-fidelity gaussian process based empirical potential development for si: H nanowires. *Theoretical and Applied Mechanics Letters*, 10(3):195–201, 2020.
- [22] D. P. Kingma and J. Ba. Adam: A method for stochastic optimization. *arXiv preprint arXiv:1412.6980*, 2014.
- [23] S. Lanthaler, S. Mishra, and G. E. Karniadakis. Error estimates for deeponets: A deep learning framework in infinite dimensions. *Transactions of Mathematics and Its Applications*, 6(1):tnac001, 2022.
- [24] G. Li, C. Moya, and Z. Zhang. On learning the dynamical response of nonlinear control systems with deep operator networks. *arXiv preprint arXiv:2206.06536*, 2022.
- [25] J. Li, M. Yue, Y. Zhao, and G. Lin. Machine-learning-based online transient analysis via iterative computation of generator dynamics. In *2020 IEEE International Conference on Communications, Control, and Computing Technologies for Smart Grids (SmartGrid-Comm)*, pages 1–6. IEEE, 2020.
- [26] G. Lin, C. Moya, and Z. Zhang. Accelerated replica exchange stochastic gradient langevin diffusion enhanced bayesian deeponet for solving noisy parametric pdes. *arXiv preprint arXiv:2111.02484*, 2021.
- [27] L. Lu, P. Jin, G. Pang, Z. Zhang, and G. E. Karniadakis. Learning nonlinear operators via deeponet based on the universal approximation theorem of operators. *Nature Machine Intelligence*, 3(3):218–229, 2021.
- [28] F. Milano. *Power system modelling and scripting*. Springer Science & Business Media, 2010.

- [29] G. S. Misyris, A. Venzke, and S. Chatzivasileiadis. Physics-informed neural networks for power systems. In *2020 IEEE Power & Energy Society General Meeting (PESGM)*, pages 1–5. IEEE, 2020.
- [30] C. Moya and G. Lin. Dae-pinn: a physics-informed neural network model for simulating differential algebraic equations with application to power networks. *Neural Computing and Applications*, pages 1–16, 2022.
- [31] C. Moya and G. Lin. Fed-deeponet: Stochastic gradient-based federated training of deep operator networks. *Algorithms*, 15(9):325, 2022.
- [32] C. Moya, S. Zhang, M. Yue, and G. Lin. Deeponet-grid-ug: A trustworthy deep operator framework for predicting the power grid’s post-fault trajectories. *arXiv preprint arXiv:2202.07176*, 2022.
- [33] B. Palmer, W. Perkins, Y. Chen, S. Jin, D. Callahan, K. Glass, R. Diao, M. Rice, S. Elbert, M. Vallem, et al. Gridpacktm: A framework for developing power grid simulations on high-performance computing platforms. *The International Journal of High Performance Computing Applications*, 30(2):223–240, 2016.
- [34] B. Park, K. Sun, A. Dimitrovski, Y. Liu, and S. Simunovic. Examination of semi-analytical solution methods in the coarse operator of parareal algorithm for power system simulation. *IEEE Transactions on Power Systems*, 36(6):5068–5080, 2021.
- [35] A. Paszke, S. Gross, F. Massa, A. Lerer, J. Bradbury, G. Chanan, T. Killeen, Z. Lin, N. Gimelshein, L. Antiga, A. Desmaison, A. Kopf, E. Yang, Z. DeVito, M. Raison, A. Tejani, S. Chilamkurthy, B. Steiner, L. Fang, J. Bai, and S. Chintala. PyTorch: An Imperative Style, High-Performance Deep Learning Library. In H. Wallach, H. Larochelle, A. Beygelzimer, F. d’Alché Buc, E. Fox, and R. Garnett, editors, *Advances in Neural Information Processing Systems 32*, pages 8024–8035. Curran Associates, Inc., 2019.
- [36] T. Qin, Z. Chen, J. D. Jakeman, and D. Xiu. Data-driven learning of nonautonomous systems. *SIAM Journal on Scientific Computing*, 43(3):A1607–A1624, 2021.
- [37] T. Qin, K. Wu, and D. Xiu. Data driven governing equations approximation using deep neural networks. *Journal of Computational Physics*, 395:620–635, 2019.
- [38] M. Raissi, P. Perdikaris, and G. E. Karniadakis. Multistep neural networks for data-driven discovery of nonlinear dynamical systems. *arXiv preprint arXiv:1801.01236*, 2018.
- [39] M. Raissi, P. Perdikaris, and G. E. Karniadakis. Physics-informed neural networks: A deep learning framework for solving forward and inverse problems involving nonlinear partial differential equations. *Journal of Computational physics*, 378:686–707, 2019.
- [40] S. Ross, G. Gordon, and D. Bagnell. A reduction of imitation learning and structured prediction to no-regret online learning. In *Proceedings of the fourteenth international conference on artificial intelligence and statistics*, pages 627–635. JMLR Workshop and Conference Proceedings, 2011.
- [41] P. W. Sauer, M. A. Pai, and J. H. Chow. *Power system dynamics and stability: with synchrophasor measurement and power system toolbox*. John Wiley & Sons, 2017.
- [42] H. Schaeffer. Learning partial differential equations via data discovery and sparse optimization. *Proceedings of the Royal Society A: Mathematical, Physical and Engineering Sciences*, 473(2197):20160446, 2017.

- [43] J. Shu, W. Xue, and W. Zheng. A parallel transient stability simulation for power systems. *IEEE Transactions on Power Systems*, 20(4):1709–1717, 2005.
- [44] B. Stott. Power system dynamic response calculations. *Proceedings of the IEEE*, 67(2):219–241, 1979.
- [45] M. A. Tomim, J. R. Marti, and L. Wang. Parallel solution of large power system networks using the multi-area thévenin equivalents (mate) algorithm. *International Journal of Electrical Power & Energy Systems*, 31(9):497–503, 2009.
- [46] S. Wang and P. Perdikaris. Long-time integration of parametric evolution equations with physics-informed deepnets. *arXiv preprint arXiv:2106.05384*, 2021.
- [47] S. Wang, H. Wang, and P. Perdikaris. Learning the solution operator of parametric partial differential equations with physics-informed deepnets. *Science advances*, 7(40):eabi8605, 2021.
- [48] T. Wang, X. Bao, I. Clavera, J. Hoang, Y. Wen, E. Langlois, S. Zhang, G. Zhang, P. Abbeel, and J. Ba. Benchmarking model-based reinforcement learning. *arXiv preprint arXiv:1907.02057*, 2019.
- [49] Y. Wang and G. Lin. Mfpc-net: Multi-fidelity physics-constrained neural process. *arXiv preprint arXiv:2010.01378*, 2020.
- [50] Y. Yang, G. Kissas, and P. Perdikaris. Scalable uncertainty quantification for deep operator networks using randomized priors. *arXiv preprint arXiv:2203.03048*, 2022.